Nanofibrous MgO Composites: Structures, Properties and Applications

Tuğba Baysal[1,2], Nuruzzaman Noor[3], Ali Demir[4]

[1]MSc Student at Istanbul Technical University, Nanoscience and Nanoengineering Programme, Istanbul-Turkey

[2]Research Assistant at Burdur Mehmet Akif Ersoy University, Department of Nanoscience and Nanotechnology, Burdur-Turkey

[3]Research Assistant Professor at The Hong Kong Polytechnic University, Institute of Textiles and Clothing, Hong Kong

[4]Prof. Dr. at Istanbul Technical University, Department of Textile Engineering, Istanbul-Turkey

(Corresponding Author: ademir@itu.edu.tr)

ABSTRACT

Nanomaterials have become an established area of academic research and they have gained commercial importance due to their valuable physico-chemical properties, such as large surface area, high mechanical strength as well as unique optical and electrical features. Numerous nanosize architectures have been researched and reported to date including quantum dots, fullerenes, nanorods, nanowires, nanofibers, nanosheets, nanowalls, nanocoils and nanoballs etc. Among these materials, nanofibers are extremely valuable morphologies used across many industries spanning from textile to medical applications and beyond. This review article has focused on the various works and reports of MgO-based applications and its overlap with nanofiber-based structures – a growing area of industrial and academic interest. A comprehensive review of the growing number of reports to date was carried out, so as to provide a unified resource for researchers going forward. As the acceptance and broader set of applications continues its exponential growth in commercial and academic output, it is envisaged that MgO-based composites will play a central part in many future reports of nanofibrous composites (and broader composite), due to the wide variety of applications to which MgO is suited, as well as other peripheral properties such as cost, availability, ease-of-handling and use etc. Indeed, despite the many preliminary reports to date, there remains a great deal yet to discover and optimise for such systems.

1. An Introduction to Nanofibers and MgO-based Composites

Nanomaterials have become established areas of academic research and commercial importance due to their valuable (and often fascinating) physico-chemical properties, e.g.; large surface area, high mechanical strength as well as unique optical and electrical features. Numerous nanosized architectures have been reported to date including quantum dots, fullerenes, nanorods, nanowires, nanofibers, nanosheets, nanowalls, nanocoils and nanoballs etc. Among these materials, nanofibers are extremely valuable morphologies used across many industries spanning from textile to medical applications and beyond [1–5].

Nanofibers (NF) are 1D structure with diameters below 1 μm and high specific surface area that can reach 1000 m^2/g. Nevertheless, extremely long lengths, up to the range of metres, can be achieved (Figure 1). This morphology affords extremely valuable properties such as high surface area to volume ratio, low density, high porosity and flexibility. It also means that NF find wide applications in areas including cosmetics, drug delivery carrier, wound dressing, membranes and filters for all purposes including bio/chemical warfare gases, biochemical sensors, electronic devices and tubes for blood vessels [6–11].

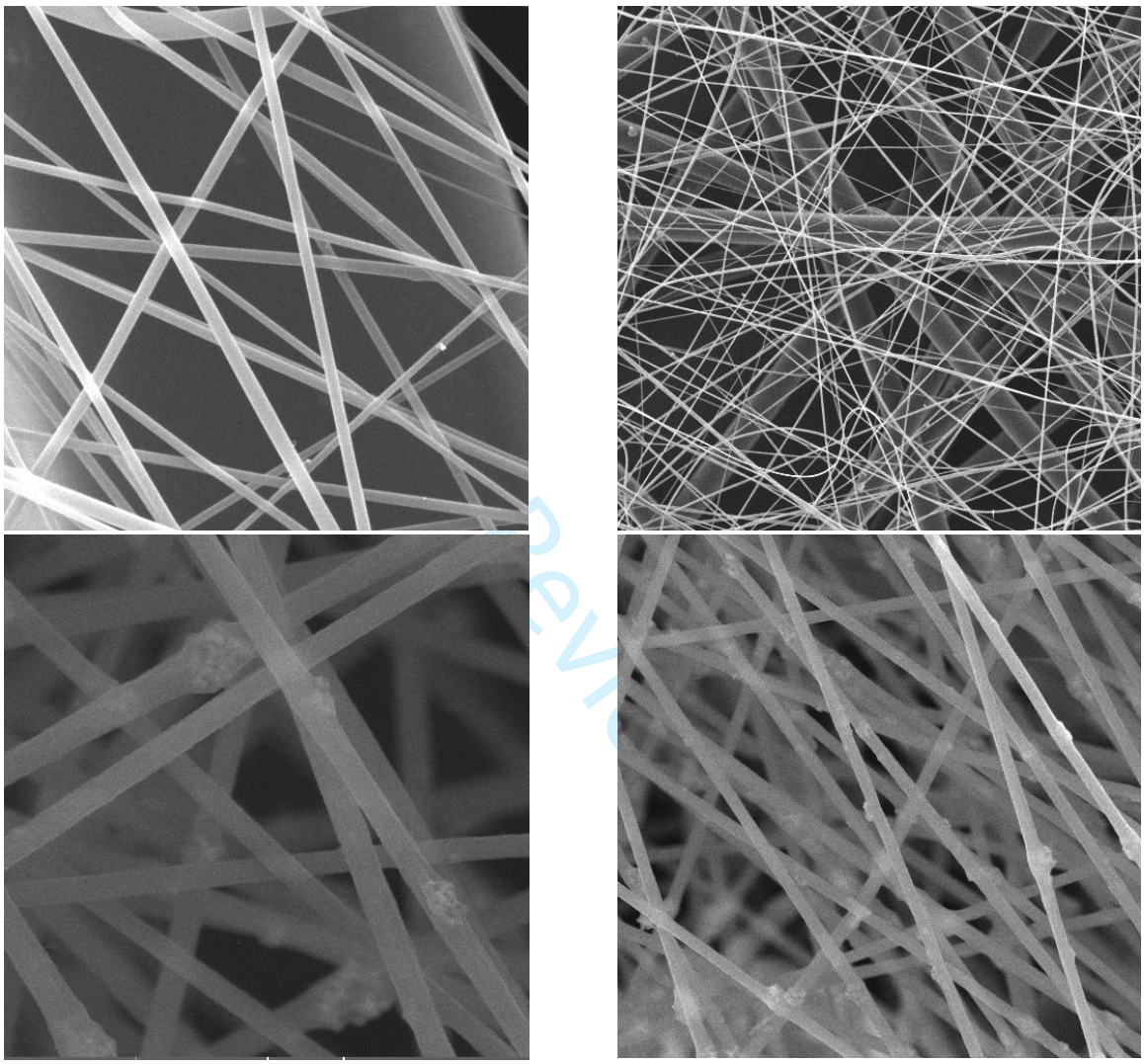

Figure 1. Electrospun nanofibers under SEM with different magnification. The SEM pictures have been taken by the authors to show the diversity of the nanofibers with their smooth, flexible, multi faceted (embedded with nano particles) nature.

First produced by William Gilbert (1544-1603) who observed that when a water droplet on a dry surface was exposed to an electrically-charged amber mineral, it turned into a cone shape, now referred to as a *Taylor Cone* [12,13]. Subsequently, luminaries such as Lord Rayleigh, Charles Vernon Boys, John Francis and Anton Formhals further developed and progressed the field of electrospun NF, although contemporary interest in the electrospinning field was re-ignited and popularized by Doshi and Reneker from 1995 onwards [14]. Based on this and related methods, various polymer, inorganic and composite nanofibrous architectures have

been composed including support materials such as Au, Ag, TiO_2, MgO, MnO_2 Al_2O_3, ZnO and Fe_2O_3.

Magnesium oxide (MgO), much like other inorganic metal oxides, tends to be chemically and thermally stable under even harsh process conditions whilst also exhibiting excellent biocompatibility, biodegrading into soluble Mg^{2+}, non-toxic by-products (indeed it is the second most abundant intracellular cation and an essential metabolic nutrient e.g.; for cellular respiration, protein synthesis, membrane integrity, effective function of nerve tissue, and in repairing nerve damage as well as in bone remodelling and skeletal development, ATPase function and oxidative phosphorylation etc.) [15–17]. Such inorganic structures have been explored with a view to generally improved properties of biodegradability, hydrophobicity, photocatalytic effects, electrical conductivity, etc., as well as more specific applications such as biological sensing, capacitors, filtration of volatile organic compounds, photocatalysis and energy generation storage [18,19].

For example, Au, Ag and TiO_2 have been used in NF for many years to improve antibacterial, catalytic, chemical and heat resistance properties. MgO has become increasingly popular in recent years due to its low cost (of precursors), relative abundance, biocompatibility (Mg^{2+} is essential to human metabolism and naturally found in bone tissues and used in regeneration) and environmentally-benign nature [20,21]. The shape and size of nanocrystalline MgO nanoparticles (NP) endow them with high specific surface and reactivity, owing to the high concentration of edge/corner sites and structural defects on their surface [22]. MgO shows high adsorption capacity for heavy metals and toxic gases, native antimicrobial property, non-toxicity, biocompatibility and thermal and electrical insulation. Embedding of MgO nanoparticles in NF, or using them as dopant components, allows for enhanced activity bactericides, filters, ceramic materials, refractory properties and catalytic activity (Figure 2) [23–28].

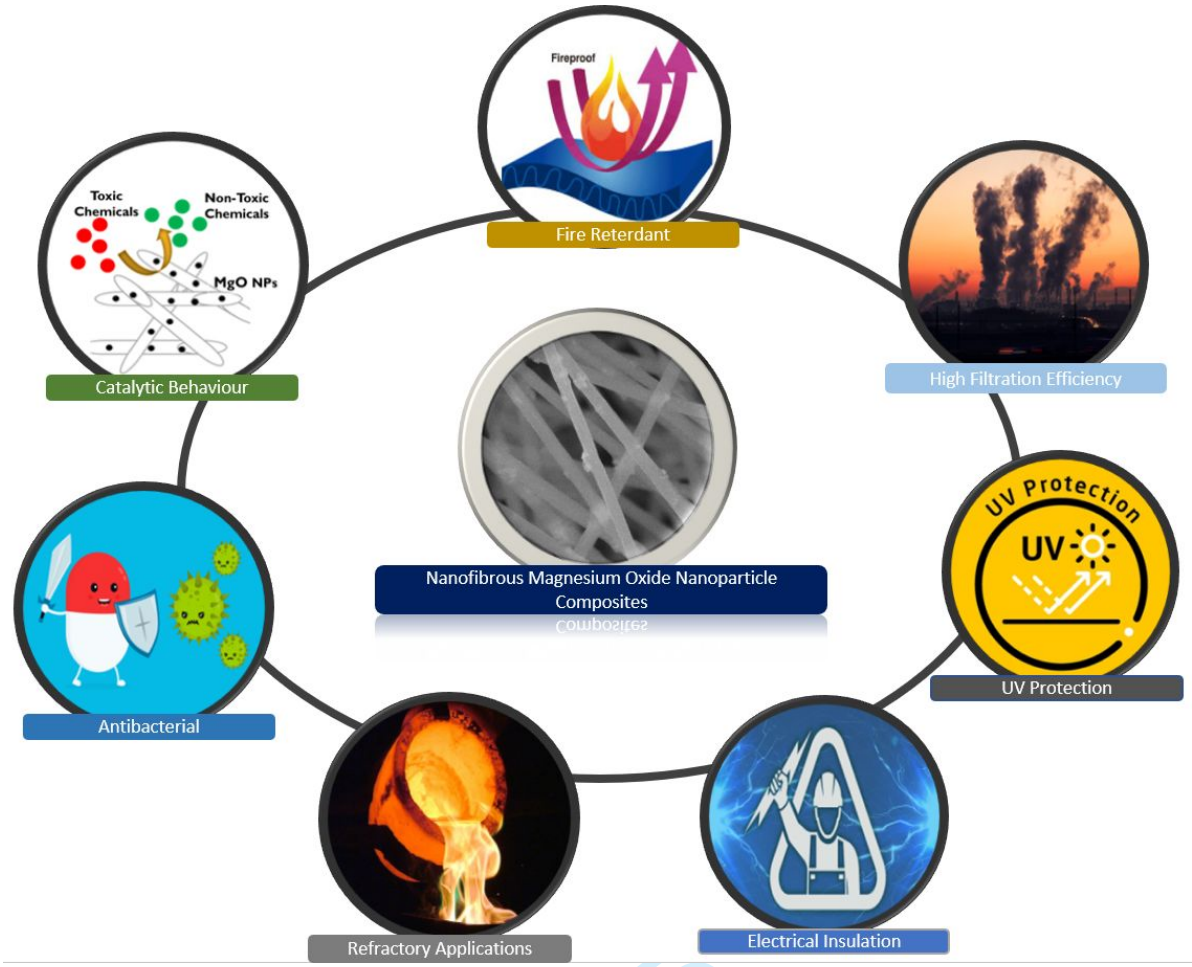

Figure 2. Illustrative overview of the broad number of potential applications of nanofibrous MgO nanoparticle composites

As such, MgO-based materials will play a critical role as the broader NF-based academic and commercial outputs continue to grow in relative volume, applications and importance. The aim of this review article is to provide a comprehensive overview of MgO-based NF, including NF synthesis strategies, as well as the numerous applications of such flexible, multifunctional composites.

1.1 An Overview of Nanofiber Synthesis Methods Suited to MgO-based Composite Formation

The production of advanced NF can occur through a variety of methods. An overview of such processes is given in

Table **1**.

Table 1. Overview and appraisal of some of the most widely used nanofiber production methods

Method	Process	Drawback	Reference
Drawing	Nanofibers are mechanically drawn from polymeric liquids	Only viscoelastic polymers can be used	29
Template Synthesis	Nanofibers of solid or hollow architectures are obtained using some templates (alumina or self-ordered nano-porous membrane) then nanofibers are released from these templates by mechanical processes.	Production of a continuous nanofiber is not possible	30
Self-Assembly	Individual and pre-existing components organize themselves into goal patterns.	Production time tend to be very long	31
Electrospinning	Polymer solution is spun under high voltage with direct current and the solvent evaporates till the formed nanofibers reach the collector	Low production rate, even with recent advances	32
Solution Blowing	Polymer solution and pressurized gas streams flow simultaneously, and the solvent evaporates until the formed nanofibers reach the collector	Formation of thick and beaded nanofibers	33
Centrifugal Spinning	By use of centrifugal forces, the solvent of a polymeric solution is removed and nanoscale fibers are produced	Although high production rate is achievable, bead formation is often observed	34

Among these methods, for the production of narrow sized NF, low cost, controllable process parameters via a simple synthesis process; electrospinning is the most commonly used fabrication technique. In addition, electrospinning allows process parameters (applied voltage, distance between the needle and collector, solution flow rate, viscosity, etc) to be readily varied in order to produce the desired fiber structure properties for any application [35,36], as shown in

Table **2** [37]. NF diameter in turn determines the important properties of the nanofibrous mats used in various applications, with the incorporated MgO having large impacts on the eventually output electrospun fiber diameter. For example, in certain cases where a more conductive electrospinning solution facilitates faster acceleration of jetting, it overcomes the effect of higher viscosity and higher NF diameters are expected [37].

Table 2. Electrospinning parameters for nanofiber synthesis and their effects on the fiber morphology *(adapted from Zhu et al)*[38]

PARAMETERS		Fiber Morphology
Solution Parameters	*Solution Concentration & Viscosity*	**Low:** Decrease in fiber diameter, Bead generation [39–41] **High:** Increase in fiber diameter and uniform fiber morphology without beads [39–41]
	Conductivity	**Low:** Bead generation [42] **High:** Decrease in fiber diameter and uniform fiber morphology without beads [42]
Process Parameters	*Applied Voltage*	The effect of applied voltage on nanofiber diameter is not very clear [43–45]
	Flow Rate	**High:** Increase in fiber diameter, Bead generation [46,47] **Low:** Decrease in fiber diameter [46,47]
	Needle to Collector Distance	**High:** Decrease in fiber diameter [44]
	Time	**High:** Increase in packing density and solidity of fiber and decrease in pore size among fibers [48,49]
Ambient Parameters	*Temperature*	**High:** Decrease in fiber diameter [50]
	Humidity	**High:** Increase in the number, diameter, and distribution of pores [51]

2. *MgO Composite Properties and Applications*

2.1 Adsorption Properties of MgO Functionalized Nanofibers for Filtration Applications

It is argued that approximately 40% of deaths worldwide are caused by pollution, and this number is projected to increase as the growing output of pollutants in the air, water and soil remains unchecked [52]. Pollutants, in their variant forms, must be removed in order to improve liveability, quality-of-life and to protect long-term health. Solid and liquid contaminants can be removed by conventional membrane or filtration technology while gases pose a greater challenge [53].

Volatile Organic Compounds (VOC) pose an especially difficult problem. VOC are classified as chemical substances with a vapor pressure of more than 10 Pa at 293 K by the European Union (EU) and potentially lead to photochemical smog, carcinogenesis, teratogenesis and mutagenesis [54,55]. VOC gases can harm the human body upon long-term exposure even at very low concentrations (ppm levels). Examples of VOC are gasoline, benzene, formaldehyde and solvents such as toluene and xylene, styrene. Chemical Warfare Agents (CWA) are an especially harmful class of VOC and although banned by the Chemical Weapons Convention since 1997, they unfortunately remain easily accessible to terrorist groups or unscrupulous governments and therefore pose a major threat worldwide [56–58]. For these reasons, effective adsorbents are in great demand for the efficient and effective removal of VOC.

Airborne particles are easily trapped by nanofiber membranes (NFM), due to the small pore sizes, small fiber diameters and high surface area physical properties of such systems. By further chemically functionalising the surface of NFM, toxic gases and VOC can readily adsorb onto the NF surface. To this end, adsorbent materials such as activated carbon, zeolites or graphite can be used or metal oxides like MgO, Al_2O_3, MnO, ZnO or TiO_2 can be composited with NF to improve adsorption ability [59]. In each case, the maximum gas

adsorption capacity is closely related to the specific surface area of the material, the pore size and pore size structure, as well as the chemical affinity between the adsorbents and the VOC. Thus, the adsorbent materials must be chemically and thermally treated to form micro-sized pores that maximise the affinity and binding efficacy for the VOC of interest. As shown in Figure **Error! Reference source not found.**, the adsorbate polarity, boiling point, density and molecular structure affects adsorptive capacity [60,61].

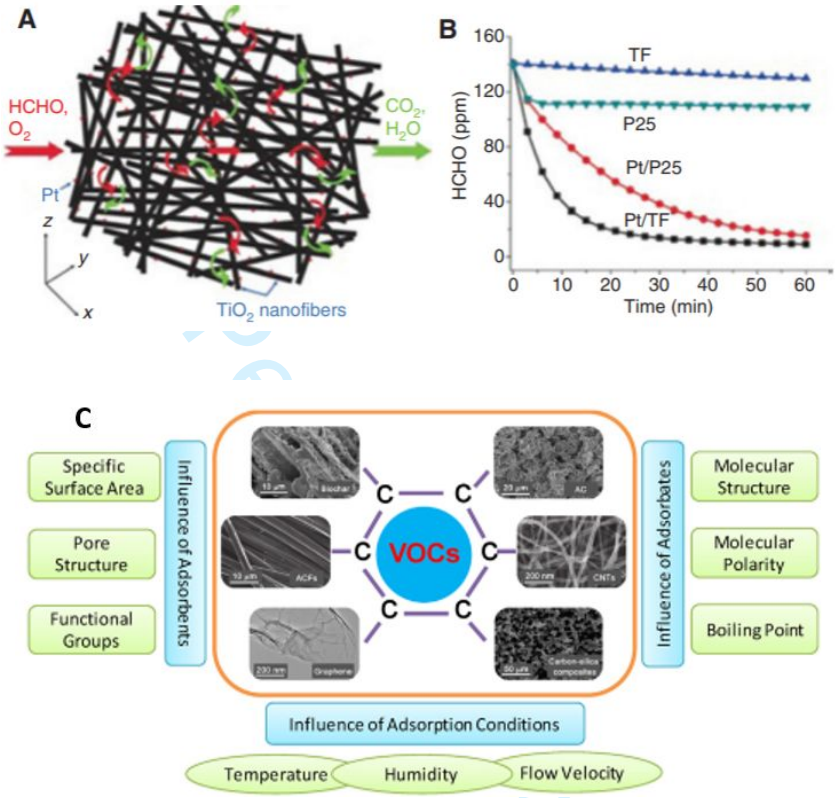

Figure 3. A) Illustration of the fast diffusion of reactants (HCHO and O_2) and products (CO_2 and H_2O) in the hierarchically porous channel of the Pt/TF catalyst *(adapted from Wang et al)* [62], B) Changes in formaldehyde (HCHO) concentration as a function of reaction time for the Pt/P25 and Pt/TF samples *(adapted from Wang et al)* [62], C) The important parameters of VOCs adsorption *(adapted from Zhang et al)*[61].

2.2 The Adsorptive and Degradative Capabilities of MgO Nanoparticles

Metal oxides such as MgO, Al_2O_3, FeO, CaO, TiO_2, R-Fe_2O_3, ZnO, and WO_3 are commonly used in industrial applications as adsorbents, catalysts and catalyst supports [63]. Due to increased surface area, high reactive edge and corner defects sites and unusually stabilized lattice planes, the reactivity of nano-sized metal oxides is higher than that of their bulk counterparts. Nazari and Jaafari confirmed that nanocrystalline MgO could destroy organophosphorus compounds due to enhanced surface reactivity [64]. So, MgO NPs are widely used in NF as a disruptive adsorbent for CWA [65]. Many functional groups such as alcohols, acids, aldehydes, ketones, and heteroatoms (e.g.; S, N and P) containing chemicals are adsorbed exothermically on the MgO surface, with often a multitude of co-ordinations possible leading to a variety of possible degradation avenues towards eventual non-toxic by-products. Disruptive adsorption is preferred because it ensures the irreversible degradation of

toxic species whereas physical adsorption ensures only reversible attachment of toxic species [66].

However, it is often difficult to effectively mount NP to clothing – leaching is a common issue with soft matter incorporation, whilst aggregation is another problem [18]. One route to avoiding mounting and dispersion problems involves adding inorganic additives, such as MgO, to a pre-polymer mixture solution and a well-dispersed, well-encapsulated composite made by various methods, including NF synthesis routes [67]. However, in such methods, the NP surfaces are coated by the polymer and therefore the efficacy across various application areas is greatly reduced due to an insufficient amount of available NP on the surface. Alternatively, NF synthesis and the subsequent addition of NP by electro-spraying onto fiber surfaces is a strategy to improve effectiveness in such applications [66].

Michalkova *et al*. [68] simulated the interaction between MgO NPs and sarin – a toxic organophosphorus compound often used as a chemical warfare agent (CWA); see Figure . $Mg_{16}O_{16}$ and Mg_4O_4 cluster models were used to examine the adsorption ability's dependence on cluster size. The calculations showed that while sarin was adsorbed in $Mg_{16}O_{16}$ by molecular physisorption, attributed to the formation of hydrogen bonds and to the ion-dipole and dipole-dipole interactions between sarin and surface of $Mg_{16}O_{16}$, chemisorption was favoured in Mg_4O_4; attributed to the formation of covalent bond between sarin and surface of Mg_4O_4. Therefore, Mg_4O_4 was proven to have superior reactivity due to irregular edges, corners, defect sites and low coordination number.

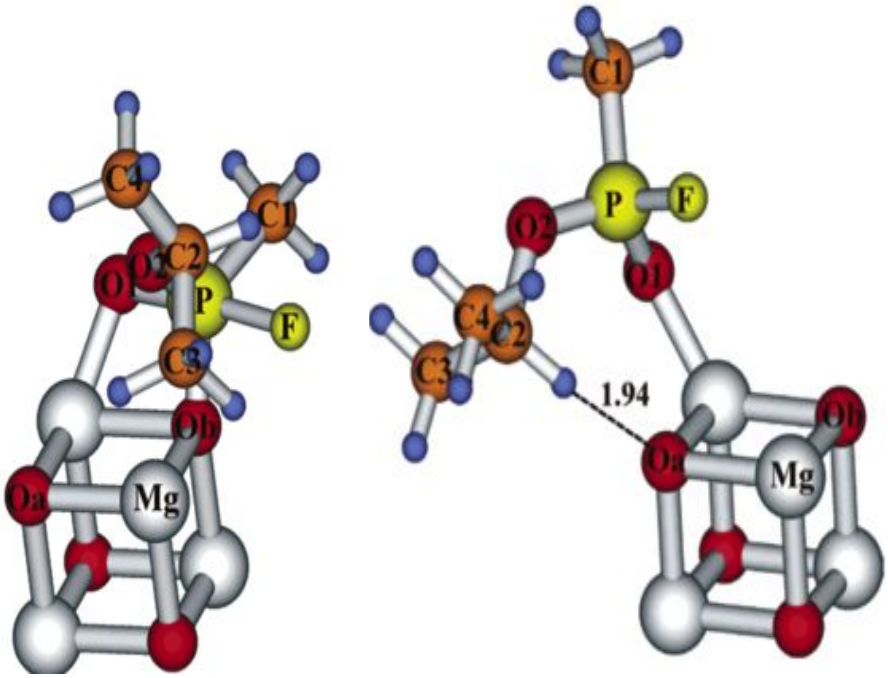

Figure 4. Schematic representation of the geometric structure of magnesium oxide (Mg_4O_4)-Sarin adsorbed system (*adapted from Michalkova et al*) [68].

In the case of hydroxylated MgO fragments, ion-dipole, dipole-dipole and hydrogen bonds form between sarin and the MgO NPs, although only physical adsorption (i.e.; non-destructive co-ordination) is predicted. This is because the energy of chemisorbed systems (-209.2 kJ/mol) is higher than physisorbed systems (~12.1 kJ/mol) such that it is difficult to remove these strong bonds from the structure and, so causes formation of a new structure. Thus, due to the lack of stronger covalent bond formation, there is no destructive adsorption predicted. However, when unhydroxylated small MgO fragments are used, strong covalent bonds can form between sarin and the MgO surface, allowing destructive adsorption via removal of the fluorine atom from sarin, to be observed. Nevertheless, a process that ensures the formation of the hydrogen fluoride (HF) by-product is necessary to decompose the sarin adsorbed onto the hydroxylated small fragment of MgO [68].

Low coordinated metal ions are more reactive and can co-ordinate materials easier than larger complexes since the magnitude of the adsorption energy is a decreasing function of the coordination number of the ions of the adsorption site. Branda *et al.* [69] studied ethanol adsorption on a perfect MgO(100) surface, and on the topologic surface defects of MgO. The ethanol molecule is adsorbed chemically on terrace sites of MgO without any removal by means of a two-fold interaction (a hydrogen bond with an $O_{substrate}$-$H_{alcohol}$ and a weaker $O_{alcohol}$-$Mg_{substrate}$ bond) while strong disruptive chemical adsorption is realized on edge and corner sites. The O-H bond of the alcohol breaks down, causing an ethoxide bound to the Mg cation and produces a surface hydroxyl on the vicinal $O_{substrate}$. Besides, the catalytic power of a metal oxide NP improves as the accessibility of the low-coordinated metal atoms in its crystalline structure increases. Moreover, higher specific surface area of the metal oxide NP leads to higher accessibility of the low-coordinated metal atoms in metal oxide NP [70].

A relationship between adsorption energy of ethanol on different site of MgO structure and adsorption type (dissociative or associative) can be established. Where the adsorption energy between the substrate and alcohol is very high, dissociative adsorption occurs because both the carbon atom and the oxygen atom in the ethanol are strongly attracted by the substrate and the O-H bond breaks down. If the adsorption energy is insufficiently high, the O-H bond is not broken and binds to the substrate by associative adsorption. According to values of adsorption energy of ethanol on MgO (step edge (coordination number (CN):4)=0.83 eV , O-apical corner (CN:3) =1.32 eV, Mg-apical corner (CN:3) = 1.82 eV); the reactivity of the adsorption sites is edge < corner and adsorption energy of ethanol having 3 or 4 CN at adsorption site is enough high for dissociative adsorption [69,71].

MgO has also been explored for its degradative effects in other noxious materials including 2-chloroethyl ethyl-sulphide (2-CEES) and cadmium (Cd (II)). Dadvar *et al.* [72] produced activated carbon nanofibers (ACNF) embedded with MgO NPs, for use in the degradation of mustard gas surrogate, 2-CEES. As the amount and specific surface area of MgO NPs onto ACNFs increase, 2-CEES adsorption rate increases. Compared to pure ACNFs, the adsorption rate of MgO-ACNFs is 2-4 times higher, depending on the specific surface area of MgO used. The MgO NPs ensure decontamination of toxic chemicals like 2-CEES from the environment via their catalytic behaviour. Similar observations were obtained by Dadvar *et al.* [73] who showed the disruptive effect of ACNF involving MgO. FTIR results indicated that produced

filters adsorb and then destroy the 2-CEES, by means of new covalent/alkoxide bonds between 2-CEES and the surface reactive oxide/hydroxyl groups of MgO-NP. Further, a higher recorded weight-loss (+21%) for the PAN NF-containing MgO NP vs. MgO-free PAN NFs may be related to high catalytic activity of metal oxide NPs and the improvement of the pyrolysis process of MgO NPs embedded in ACNFs during activation.

Behnam *et al.* [74] have similarly used ACNFs containing MgO NPs (15 wt% in the precursor mixture.) for destructive adsorption of diazinon solution, a type of synthetic pesticide that causes serious health problems in humans. After 10 minutes interaction, HPLC of the solution indicated presence of a new peak; later determined to be a 2-isopropyl 6-methyl 4 pyrimidinol (IMP) degradation by-product, by LC-MS. Furthermore, the amount of adsorbed diazinon was observed to increase rapidly up to 30 min, then slightly decreased and remained constant. Embedded metal oxide NPs in ACNFs increase the adsorption of diazinon by 15-25%, depending on the type and specific surface area of metal oxide NPs (Figure). It is known that MgO and Al_2O_3 can destroy pesticides due to the alkalinity that originates from hydroxyl groups and MgO has higher alkalinity than Al_2O_3 [75].

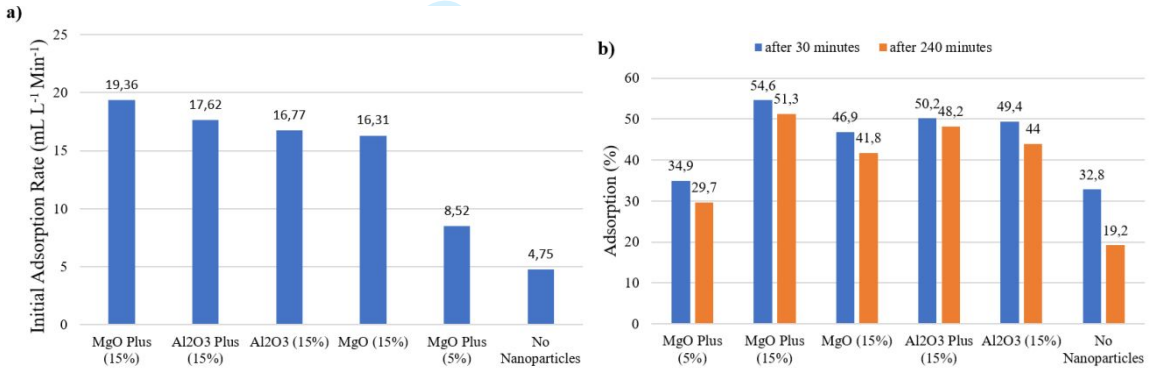

Figure 5. a) Initial adsorption rate of diazinon by ACNFs containing MgO, Al_2O_3, MgO Plus and Al_2O_3 Plus in the first 5 min after introduction of the sample to the reaction solution b) The amount of adsorbed diazinon after 30 and 240 min (*adapted from Behnam et al*)[74] .

Othman *et al.* [76] produced polyacrylonitrile (PAN)-MgO based ACNFs for methane adsorption. MgO NPs addition caused the fiber diameter to decrease from 578 nm to 520 nm and moreover specific surface area (SSA) of MgO-ACNF to increase nearly four-fold (1893 m^2/g) as compared to pristine ACNFs (478 m^2/g). It also improved adsorption properties such as SSA, micro-mesopore volume and pore size (Table 3); the MgO-ACNF adsorbed higher amount of CH_4 than pristine ACNFs (2.37 mmol/g, 1.49 mmol/g respectively).

Table 3. Textural properties of pristine ACNFs and ACNFs embedded with MgO *(adapted from Othman et al)*[76].

Samples	BET S.S.A. (m^2/g)	Pore size (cm^3/g)	Total Pore Volume (cm^3/g)	Micro Pore Volume (cm^3/g)	Meso Pore Volume (cm^3/g)
ACNF	478	0.1938	0.2097	0.1593	0.0504
ACNF MgO	1893	0.7336	0.6212	0.5340	0.0872

Yusof *et al*. [77] also produced ACNFs embedded with MgO NPs. Higher SSA in composites were observed vs. pure ACNFs, i.e; 198.80 m^2/g vs. 15.43 m^2/g. The resultant surface morphology was rough due to the distribution of MgO NPs onto the ACNF surface. Furthermore, in the production of ACNFs, heat treatment is applied and yields a micro-/mesoporous structure due to formation and subsequent release of CO and CO_2 gas; the density of micropores increasing with increasing addition of MgO NPs. This in turn increases the total SSA and improves adsorption performance on the surface of ACNFs. In this study, Yusof *et al.* [77] found that Cd(II) adsorption on MgO-ACNFs is higher than pure ACNFs and granular activated carbon (GAC).

Hussain *et al*. [78] covered activated carbon fabric (ACF) with PEO-MgO NPs by electrospinning and investigated its toluene adsorption at 30℃. They found that the metal oxide NF composites (33% toluene adsorption) have higher adsorption capacities than that of ACF (31% toluene adsorption) alone.

Bo Ren [79] produced $Mg(NO_3)_2$ NF via electrospinning. After calcination process at 500℃, MgO NF was obtained and used as an adsorbent to remove highly toxic uranium (VI). It was found that the maximum adsorption occurred at pH 6, the equilibrium adsorption amount was ~90 mg/g, and the equilibrium time was 120 min.

Combination of MgO with PPG have given promising result for heavy metal adsorption [23]. Almasian *et al*. [23] synthesized a new monomer containing HEMA (2-hydroxyethyl methacrylate), IPDI (isophorone diisocyanate) and PPG (polypropylene glycol) polymerized on the surface of MgO as an adsorbent for removal of heavy metal ions from solutions. They evaluated the adsorption capacity of samples by using the Langmuir isotherm model and results are shown in Table 4. PPG seemingly has significant effects on heavy metal adsorption due to the large amounts of anionic oxygen atoms present in its structure and also its higher amount in the monomer, which can interact with the cationic heavy metals. In fact, the main mechanism for heavy metal adsorption is the intercalation of lone-pair electrons of atoms such as nitrogen and oxygen in the vacant orbitals of heavy metals. With increasing PPG content in the covered layer, the adsorption capacity increased to a certain value and then decreased. The reduction of the adsorption capacity is due to the blocking of the pores among the NF.

Table 4. A) The maximum adsorption capacity of different synthesized nanofibers *(adapted from Almasian et al)*[23], B) Langmuir and Freundlich isotherm parameters for single and competitive adsorption of Cd(II) and Pb(II) on MgO nanoparticles *(adapted from Xu et al)*[25].

A)

Adsorbent	MgO (mg/g)	MgO/PPG/0.15 (mg/g)	MgO/PPG/0.2 (mg/g)	MgO/PPG/0.35 (mg/g)	MgO/PPG/0.45 (mg/g)	MgO/PPG/0.55 (mg/g)
Pb (II)	378.58	1966.85	2377.75	1010.33	271.1	60.37
Cd (II)	270.11	1800.25	2181.75	982.31	213.68	51.37
Cu (II)	311.47	1828.64	2280.5	995.15	226.43	52.81

B)

	Metal		Langmuir			Freundlich		
		q_e, exp	q_{mL}	K_L	R^2	K_F	1/n	R^2
Single adsorption	Pb*	2983.4	3340.5885	3.1435	0.9682	2512.6167	0.4040	0.8177
	Pb**	2973.6	3332.3130	0.5086	0.9964	916.3698	0.9094	0.9190
	Cd*	1824.0	2385.4635	0.1841	0.9509	464.9966	0.2704	0.9486
	Cd**	1635.2	2214.5576	0.2323	0.9153	434.1065	0.2526	0.9124
Competitive adsorption	Pb*	1477.0	1643.8090	1.6799	0.9791	869.4928	0.4783	0.8420
	Pb**	1439.3	1737.2245	0.7152	0.9043	617.9392	0.3467	0.8068
	Cd*	1145.1	1623.5207	0.4289	0.9517	465.1361	0.2291	0.9561
	Cd**	894.5	1359.8564	0.4272	0.9852	391.3139	0.1891	0.9821

*MgO/PPG/0.15 means total weight of sample is 0.15 grams, q: adsorption capacity

A similar study of heavy metal adsorption by Xu *et al*. [25] showed that owing to higher SSA (232.4 m^2/g) and total pore volume (0.560 cm^3/g) of obtained MgO ceramic fiber, Pb(II) and Cd(II) among heavy metals, are significantly adsorbed on the ceramic MgO fiber (see Table 4). In the adsorption of Pb^{2+} and Cd^{2+} on mesoporous MgO ceramic fiber, first Pb^{2+} and Cd^{2+} are precipitated with OH^-, then ion exchange realises between Pb^{2+} and Cd^{2+} ions and Mg^{2+} or acid type OH^-.

2.3 Filtration Applications of MgO-based Nanofibers

Among air pollutants, the most dangerous particles are particulate matter 2.5 (i.e.; PM-2.5; ultra-fine pollutants with aerodynamic diameters ≤2.5 μm) [80], because they can pass through respiratory tract defence systems to readily settle into the lungs and even reach the blood circulatory systems. Serious health problems like lung cancer often result. As such, there is a great need for these materials must be filtered and removed [81].

Airborne particles are easily trapped by nanofiber membranes (NFM) due to their small pore sizes, small fiber diameters and high surface area. The morphology and size of NF can significantly affect the filtering efficiency of the resulting membrane [38]. Fiber diameter mainly affects the filtration efficiency. Smaller fiber diameters generally tend towards reduced pore size, resulting in filtration efficiency and pressure drop increases [82]. To overcome the high pressure that results, the number of pores should be higher. As a result, high filtration performance and low pressure drop, requires low fiber diameter, high number and small pores.

Sundarrajan and Ramakrishna [18] used MgO-NPs for the hydrolysis of the CWA paraoxon; a debilitating nerve agent that causes serious health problems for humans (Figure a). Exposure to paraoxon results in excessive acetylcholine activity and advanced glutamate release. This can result in seizures, excitotoxicity, and brain damage. These synaptic events associated with acetylcholinesterase inhibition are illustrated in Figure b [83]. Nanocomposite membranes were

produced by mixing of MgO-NPs with different polymers such as PVC (poly(vinyl chloride), PVDF (poly(vinylidene fluoride-co-hexafluoropropylene)) co-polymer and PSU (polysulfone) by electrospinning. For hydrolysis of paraoxon, the order of the reactivity of the membranes was found to be PVC-MgO < PVDF < PSU < PVDF-MgO < PSU-MgO. The observed low reactivity of PVC-MgO was thought due to the reaction of MgO with chlorine group in PVC. Thus, PSU was chosen as a proper polymer for this process. Moreover, comparison of the PSU-MgO (35 wt% MgO in the solution) composite with charcoal and pure MgO NPs for the hydrolysis of paraoxon was found to have 2-fold higher reactivity than charcoal, 60% lower than pure MgO NPs.

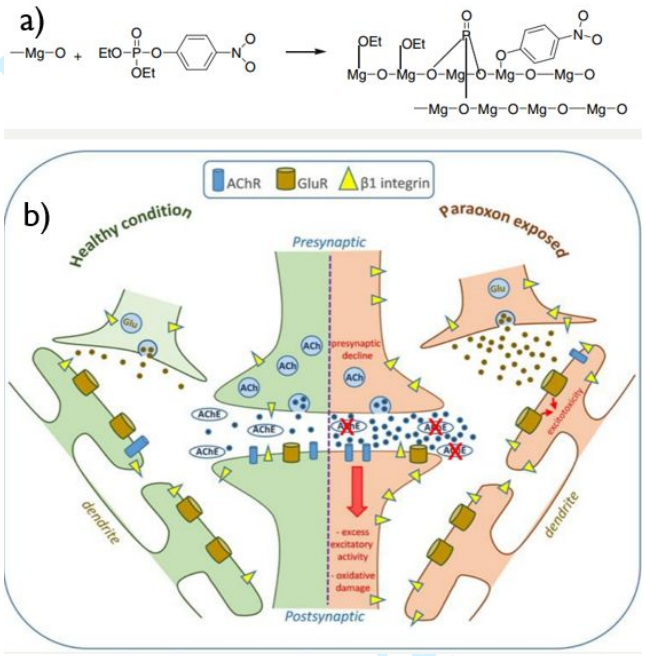

Figure 6. a) Decomposition mechanism of paraoxon on MgO surface (*adapted from Sundarrajan and Ramakrishna*)[18] b) Schematic representation of paraoxon-induced cell disorders in brain tissue (*adapted from Farizatto and Bahr*)[83].

Wei *et al.* [84] performed a similar study on the destructive adsorption of paraoxon-ethyl toxin on a hierarchical organic-inorganic nanocomposites membrane (MgO-PES-PDA NF). The MgO_{10}-PES-PDA filter and the MgO_{20}-PES-PDA filter have a relatively large SSA (54.2 m^2/g and 55.3 m^2/g, respectively), which allows the diffusion, trapping and destruction of paraoxon molecules into the pores. However, MgO_{10}-PES-PDA filter has a higher pore volume distribution with smaller pore diameters than MgO_{20}-PES-PDA. Compared to the MgO_{20} sample, the MgO_{10} sample had a smaller particle size (10.7 nm vs 27.0 nm) and a higher SSA (142.4 m^2/g vs. 53.3 m^2/g). So, the rate of active sites on the surface to that in the bulk crystal of MgO_{10} is greater than MgO_{20} thanks to its stronger size-dependency effect and thus, the MgO_{10}-PES-PDA filter has a rapid capture and large destructive capacity against paraoxon-ethyl toxin degradation with a relatively short interaction time (up to 92% in 40 min).

Sellik *et al.* [85] reported that paraoxon degradation was related to both particle size and arrangement of the MgO nanopowder used. Of the two different forms of MgO, the MgO-1 had a particle size of 11 nm arranged in a sheet, and MgO-2 of particle size of 25 nm and a

more irregular morphology not arranged in a sheet. As particle size increased, paraoxon degradation decreased (from 89.7% to 19.5%). Moreover, it appears that the arrangement in a sheet permits a higher surface area and increases the catalytic effect.

Dehghan *et al.* [86] explored the optimal electrospinning parameters such as solution concentration, distance between need tip and collector and applied voltage, for air filtration. The produced MgO-PAN composite filter was compared for variation in fiber size and porosity of filters. The most important parameter was found to be solution concentration over fiber size; as solution concentration increases, so does fiber size. MgO added to the solution increased the conductivity of the solution and also increased the solution concentration. Under normal conditions, increasing the conductivity of the solution leads to the formation of fine fibers and the concentration of the solution leads to the formation of thick fibers. A small addition to the solution can change the properties of the final product. Here, the increase in conductivity was predominant, leading to a reduction in fiber diameter as a result of MgO addition. An optimised filter media, comprising ten-layers, achieved 99.97% efficiency to collect 0.3 μm particles, similar to a HEPA filter, but with the added benefit of lower pressure drops at any flow rate compared to traditional HEPA filters. By increasing the number of layers, low pressure-drop was obtained, and high filtration efficiency was achieved.

2.4 Thermal and Mechanical Properties and Applications of Nanofibrous MgO Composites

Metal oxide fibers are preferred as refractory materials owing tostable and reliable combination of properties; high melting point, high thermal resistance and excellent oxidation resistance [87]. MgO has the highest melting temperature (2850°C) of all metal oxides and also shows excellent physicochemical properties such as lighter molecular weight (40.3 g/mol), theoretical lower density (3.58 g/cm^3) and no phase transition with the changing of temperature [88].

Lin *et al.* [88] produced MgO fibers by centrifugal spinning and following thermal treatment at high temperature and then MgO fiber-board was fabricated by injection molding the fiber slurry. This MgO fiber-board showed promising mechanical performance as determined by compressive strength measurement (Figure).

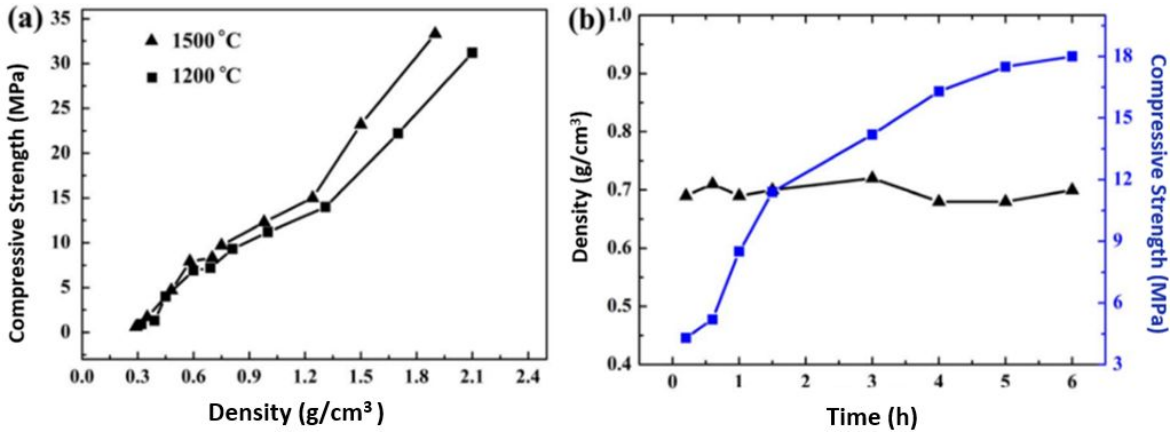

Figure 7. a) Compressive strength of MgO-based fiber-board with different density heat-treated at 1200 °C and 1500 °C respectively, b) Compressive strength of MgO-based fiber-board heat-treated at 1500 °C in different time (*adapted from X. Lin et al*)[88].

As can be seen from Figure 7a, the compressive strength of the MgO fiber-board heat-treated at 1500°C was slightly greater than heat-treated at 1200°C; with increasing temperature, mechanical properties of MgO fiber-board show only minimal change. Figure 7b, shows that as the applied heat-treatment time increases, the compressive strength of the MgO fiber-board increases, while the density of the MgO fiber-board is not significantly changed. This shows that the MgO fiber-board has high stability and promising mechanical performance at high temperatures [88].

MgO can also be used to protect against material oxidation. In an effort to solve the problem of oxidation of carbon-carbon composites, Xie and Sherwood [89] coated the surface of carbon fiber with both Al_2O_3 and MgO via a thermal evaporation method. The effect of the oxidation was monitored by exposing the fibers to oxygen ion etching at ambient temperature. Distinct functional groups that are easily observed in the valence band occurred, which can be removed by heating the fiber to high temperature. The coatings remained in the fibers even after heating and thus, these metal oxide films were proven to protect the fiber from heat and oxidation.

Owing to biocompatibility and reinforcing effect of MgO NPs, they can be used with bio-polymeric materials like chitosan membranes to improve their mechanical, thermal and barrier properties [90,91]. The chemical interaction of hydroxyl and amine groups of chitosan with MgO ensure to increase the mechanical properties [92]. The obtained chitosan/MgO composites also have thermal stability and flame-retardant properties. Silva *et al.* [90] used MgO as a nano-filler to strengthen the chitosan and showed that the tensile stress and the elastic modulus improved by 86% and 38%, respectively, compared to those of pure chitosan films by adding 5 (w/w%) of MgO. The flame retardancy (to ISO 13943 standard) demonstrated that while the burning rate of pure chitosan film was 0.2 cm/s, the burning rate of the composites containing 5 and 10 (w/w%) MgO was 0.073 cm/s. Thermal stability of nanocomposites can be seen in Figure a. The degradation temperature in all mass losses increased with the addition of MgO as compared to that of pure chitosan films. These

improvements can be attributed to the high thermal stability of MgO (as shown in Figure 8b) [93].

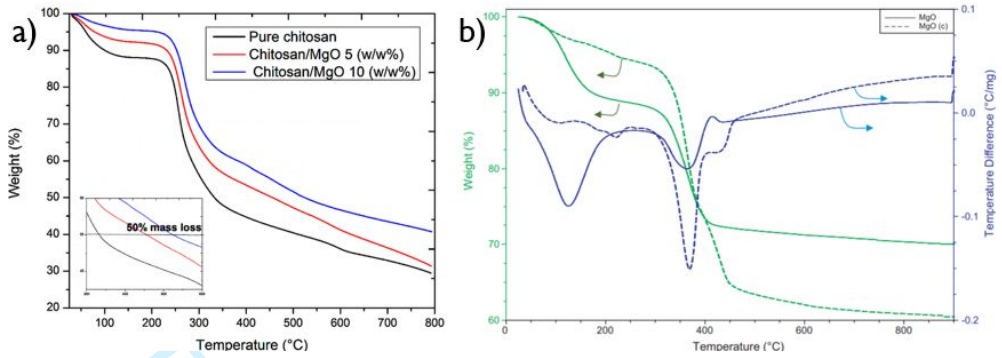

Figure 8. a) TGA curves of chitosan/MgO nanocomposites in nitrogen medium, (*adapted from De Silva et al*)[90], b) TG-DTA results of both prepared MgO and commercial MgO (*adapted from Almerindo et al*)[93].

2.5 Optical Properties/Applications of Nanofibrous MgO Composites

Although a little exposure to sunlight is beneficial for human health, sunlight also contains harmful ultraviolet radiation (i.e.; UV-A and UV-B specifically) (Figure 9a) [94], which may cause serious skin damage, eye infections etc [95]. To protect against such harmful effects, sun protective clothing that can absorb or reflect incident UV radiation can be produced, often through the use of metal oxides and metal oxide NP (e.g.; MgO, ZnO, Al_2O_3, ZrO, etc), due to their high potential in UV radiation absorption. Especially metal oxide NP have highly effective capability owing to higher specific surface area than bulk metal oxides [19]. Dadvar *et al.* [19] produced nanofibrous MgO and Al_2O_3 composites (NF were used as the substrate) and the used metal oxides had different particle diameters to indicate the effect of the specific surface area (SSA) on UV protection. They found that UV shielding capability of fiber directly related to fiber diameter. NF with small fiber diamater showed higher UV protection than usual fibers with thick fiber diameter (UV transmission of usual PAN mat was 36%, whereas NF PAN mat (748 nm) was 0.8%). This could be explained by the fact that as the NF diameter decreases, the size of the pores of the porous structure of the mat is reduced. Small pores have been shown to produce better UV-protection properties [19,96,97]. With addition of metal oxides (MgO, Al_2O_3, MgO Plus, Al_2O_3 Plus) into PAN-NF, UV transmission reduced to approximately 0.02–0.01% and MgO Plus and Al_2O_3 Plus showed higher UV protection than MgO and Al_2O_3 owing to higher SSA (Figure c,d); the higher SSA allowing more excitation of electrons in valence bands, from UV radiation. Furthermore, addition of metal oxide into NF solution cause the final diameter of NF in the mat to be reduced, thus reducing UV transmission. Finally, MgO and MgO Plus NP have higher UV protection than the Al_2O_3 and Al_2O_3 Plus NP, respectively. This may be related to the lower bandgap range of MgO (7.8 eV) compared to Al_2O_3 (8.8 eV) [19].

Silva *et al.* [90] prepared a MgO/chitosan composite and showed that pure chitosan films had very limited UV absorption compared to chitosan/MgO nanocomposite (Figure b). For example, UV absorption of chitosan nanocomposites including 5 and 10 (w/w%) MgO at 300 nm is 42% and 112% higher than the UV absorption of pure chitosan films, respectively. As a

result, UV transmission from chitosan nanocomposites is significantly reduced due to the UV protection property of MgO NP.

The optical properties of MgO was studied by Li *et al*. [98]. As a typical ionic compound, it has a wide bandwidth of 7.8 eV with high optical transmittance. The introduction of defects or color centers, such as most metal oxides, can produce an extra level in the band gap and produce strong luminescence in MgO. Pressure can create defects that prove to be a useful tool for increasing or improving the photoluminescence (PL) of wide band gap materials [98].

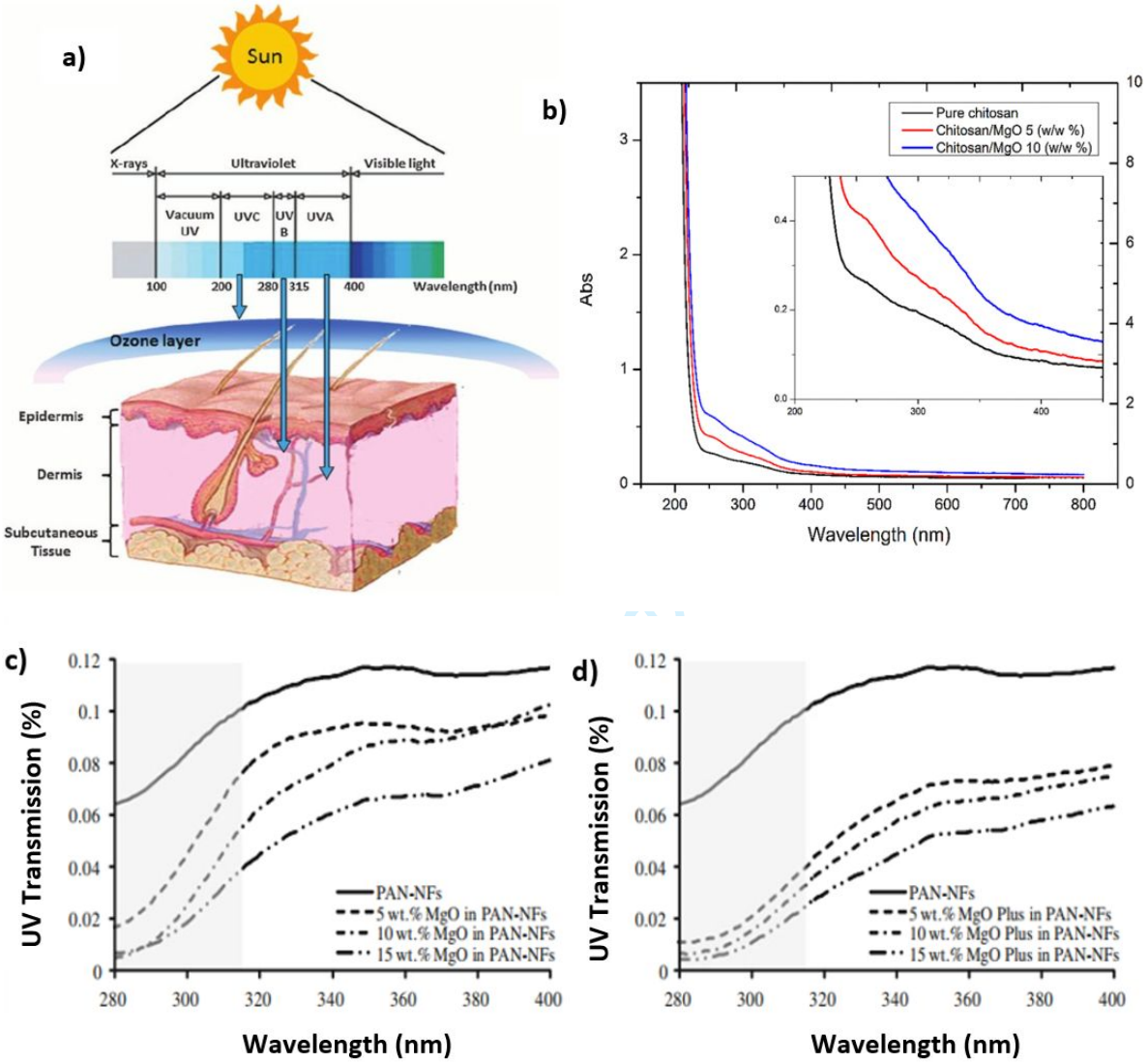

Figure 9. a) The damaging impacts of ultraviolet radaition on on skin (*adapted from Gupta et al*)[94], b) UV–vis absorption spectra of chitosan/MgO nanocomposites (*adapted from De Silva et al*)[90], c) UV transmission spectra of electrospun PAN nanofibrous mats with mat area density of 5.64 g/m^2 embedded with MgO, and d) MgO Plus (*adapted from Dadvar et al*) [19].

The PL value of MgO powder was investigated using laser excitation at 532 nm wavelength under high pressure. As can be seen Figure , the luminescence appears at about 13 GPa in the sample and has a maximum intensity of about 35 GPa. During compression, the peak of the

luminescence displays a red shift first with increasing pressure, then turns to a blue shift at ~25GPa. When the pressure was reduced to ambient pressure, PL is preserved. The researchers suggested that irreversible changes in the microstructure created by the pressure (i.e, defects and micro-strain introduced by plastic deformation of MgO) must be responsible for the observed strong luminescence [98]. These luminescent properties caused by the defective lattice of MgO can be utilized in sensor applications. Even now, it is used in IR sensor. Moreover, photoluminescent MgO may be used in designing optical material with safe, inexpensive and environmentally friendly [99]. It has been demonstrated in the literature that terbium doped MgO (MgO: Tb^{3+}) can be used as an optically stimulated luminescence (OSL) detector as an alternative to the commonly used Al_2O_3: C OSL detector [100].

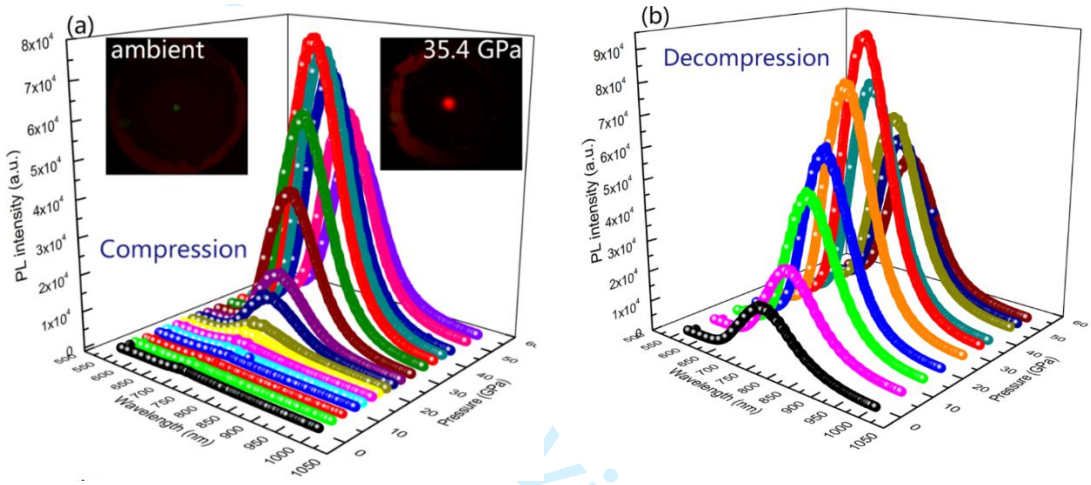

Figure 10. Photluminescence spectra of powdered MgO excited by a 532 nm laser under (a) compression, and; (b) decompression cyces. Insert micro photographs in figure (a) indicate luminescence differences at ambient and high (35.4 GPa) pressure (*adapted from X. Li et al*)[98].

2.6 Photocatalytic Activity of Nanofibrous MgO Composites

Nanofibrous MgO composites can be used to remove dye waste from industrial effluent owing to their high adsorption ability and photocatalytic degradation capability. Ordinarily, photocatalytic activity is present in semiconductor metal oxides [101–103]. Although MgO is an insulator due to its high band energy (~7.8 eV), MgO NP can be used as photocatalyst because they produce reactive species due to their natural structural defects [104].

Dyes are used across several industries such as textile, rubber, plastics, leather, cosmetics, pharmaceutical, and paper industries. Dye effluent tends to be amongst the largest environmental and societal problems caused by the textile colouration industry. If the coloured wastewater is mixed with fresh water, it reduces light penetration and photosynthesis and disrupts the aesthetic nature of the fresh-water surface [105–108]. In addition, many dyes can cause allergic dermatitis, skin irritation, abnormality of kidney, liver, brain, and the central nervous system [109]. MgO-based materials can effect degradation of low molecular weight dyes such as methylene blue (MB). Zheng *et al.* [110] prepared flower-like MgO for the degradation of MB, which completely degraded $MB_{(aq)}$ under UV irradiation (λ_{365nm}) in 90

minutes. This microstructure was more effective than other MgO morphologies (nest-like, spherical, etc.) which had longer degradation times. Thus, as the amount of MB adsorbed to MgO surface increased, due to the higher SSA, photocatalytic performance increased (Figure 1).

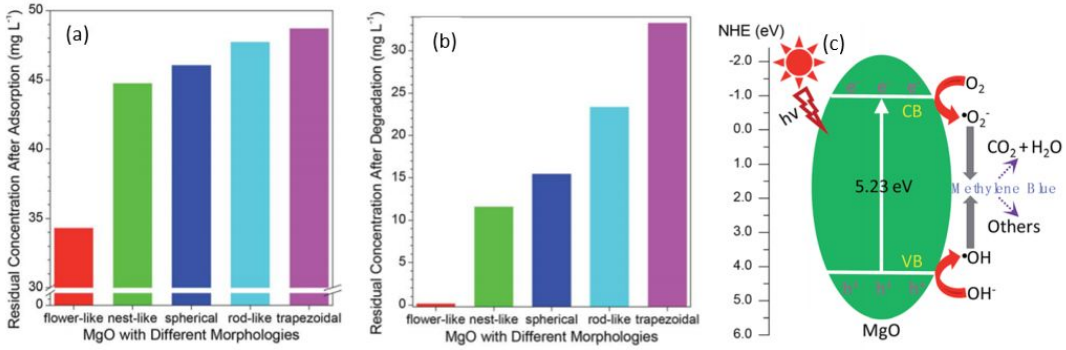

Figure 1. a) Comparison of the residual concentration of MB after adsorption of various morphologies of MgO, b) Comparison of the residual concentration of MB after photocatalytic activity of various morphologies of MgO, c) Schematic view of degradation mechanism of MB under UV irradiation (*adapted from Zheng et al*)[110].

The degradation mechanism of MB is shown in Figure 1c. Upon UV excitation, electrons in the MgO conduction band, which have a strong reducing ability, reduce the adsorbed O_2 on the surface, resulting in the formation of superoxide radical anions ($\cdot O_2^-$). In the meantime, the photogenerated holes in the MgO valence band with high oxidation potential produce more reactive $\cdot$OH radicals. The resulting radicals degrade methylene blue into CO_2, H_2O, and other by-products [110].

Mantilaka *et al.* [104] explored the photocatalytic degradation activity of electrospun nanofibrous MgO under UV irradiation against reactive yellow (RY; a widely used high molecular weight reactive dye in the textile industry). Photocatalytic degradation activity of nanofibrous MgO increased with the increase of UV irradiation time and reached 98% after 80 minutes of UV treatment and completely degraded after 100 min of UV irradiation (λ_{416nm}). Besides, this study also shows that RY dye does not degrade under UV irradiation in the absence of photocatalyst. Furthermore, the mechanism of photocatalytic degradation of dyes was clearly described as follows: MgO molecules induced by UV radiation produce reactive $\cdot$OH species and superoxide radicals by dividing the water molecules in the reaction medium. Such reactive species attack the dye molecules to break up RY dye molecules. These photocatalytic MgO NF show a great potential to be used in efficient treatment of industrial dye effluents [104].

2.7 The Dielectric Properties of MgO Functionalized Nanofibers

MgO NP is useful in isolation applications due to its dielectric properties, although such properties may vary according to the production parameters, particle size, and the synthesis method. Due to the nature of the MgO NPs, when their volume resistivity is of the order of 10^{17} Ω·m, addition of MgO NPs to the NF even at low concentrations will increase the electrical resistance of the composite [111].

The electrical resistance of MgO depends on its purity; values for high purity magnesium can reach 10^{16} Ω.m [111]. However, at high temperatures (≥2000°C), the purity does not affect electrical resistance because the temperature becomes dominant. The dielectric constant of MgO is between 3.2 and 9.8 at 25°C, and under 1 MHz, the dielectric loss values for the same conditions are about 10^{-4} [111–113]. MgO is produced as a result of the thermal calcination process of $Mg(OH)_2$ or $MgCO_3$, which also affects the surface area and pore size as well as the final reactivity of the formed MgO. Calcination should be carried out at temperatures above 1500°C to produce MgO with low chemical activity, which can be used in refractory and electrical applications [111]. For example, in high voltage insulation, MgO represents a potential filler, due to its wide bandgap (7.8 eV) and high volume resistivity (10^{17} Ω.m) – it has the highest volume resistivity value among commonly used nano-scale oxides.

Hornak *et al.* [111] used Broadband Dielectric Spectroscopy (BDS) to provide a comprehensive view of the material behavior under an electric field with a very wide frequency range, in order to show the dielectric properties of MgO. The presented test was performed in the temperature range 25 – 150 ° C and in over frequencies of 0.5 – 1 MHz, as shown in Figure 2. From the Figure 2a-b, the dielectric constant (ε') and loss factor (ε'') values increase significantly with the decreasing of measuring voltage frequency and also with increasing temperature for both cooling and heating. The main reason for the significant increase of ε' and ε'' in the highest temperature range is disordered thermal movement of particles in the MgO pellets [111]. The observed peak is a result of changes in the material structure caused by temperature rise during measurement and which significantly affect the dielectric properties of MgO [111]. Changes in the structure relate to MgO dehydration – the presence of water molecules in the composite causes a significant increase in ε' [114]. For this purpose, the NP must be dried to remove the moisture content at the surface prior to application. This was similarly reported by Pattanshetti *et al.* [115]; increasing temperature increased both ε' and ε'' of PAEK-MgO nanocomposites (Figure 12c-d).

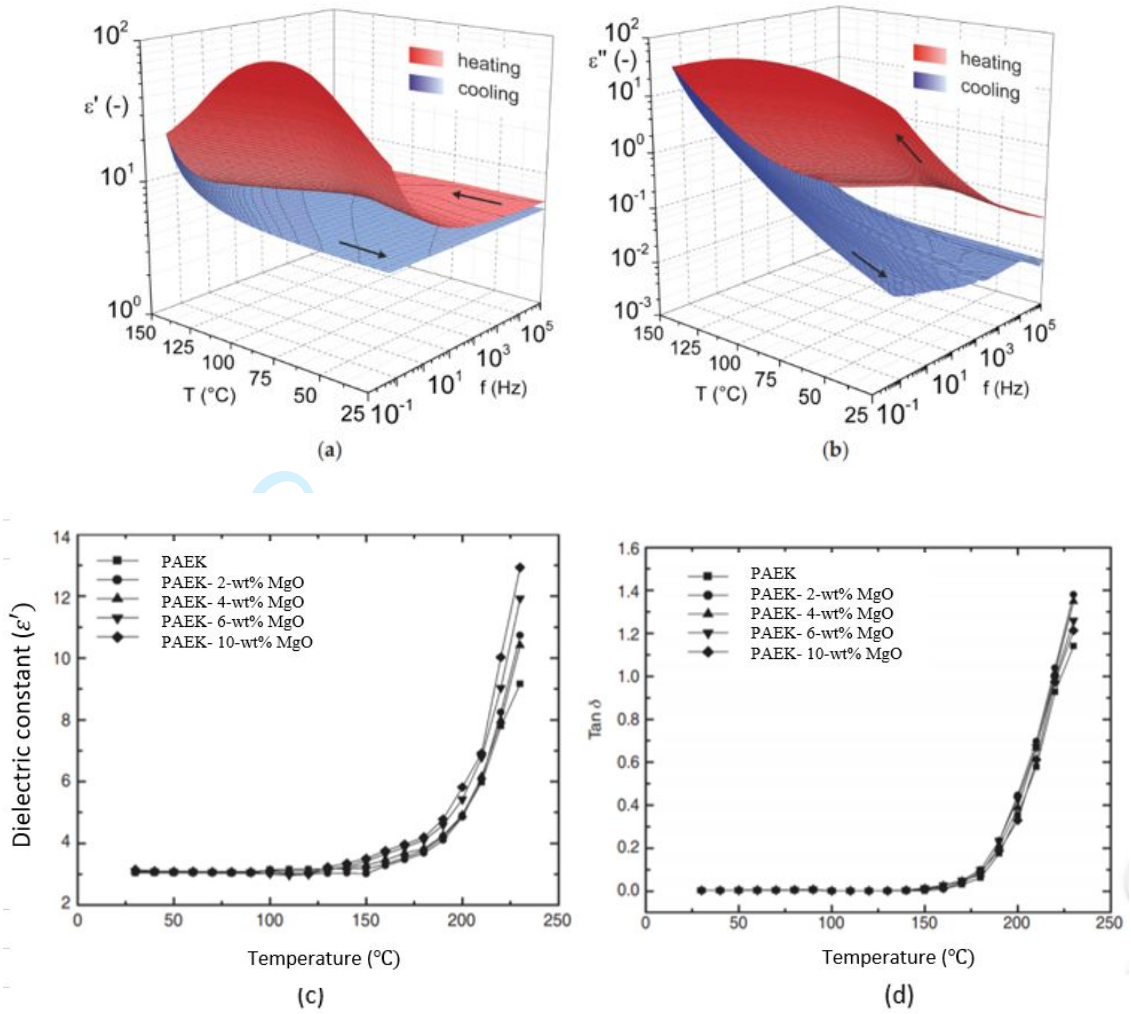

Figure 2. 3D interpretation of frequency-temperature dependencies of (a) dielectric constant and (b) loss factor for heating (red scale) and cooling (blue scale) of MgO pellets (*adapted from J. Hornak et al*)[111] ,(c) effect of temperature on dielectric constant for PAEK-MgO nanocomposites and (d) effect of temperature on tan δ for PAEK-MgO nanocomposites (*adapted from Pattanshetti et al*)[115].

Huang *et al.* [116] produced a ceramic electromagnetic absorber (EMA) composite made of short-carbon-fiber (C_{sf}) and Al_2O_3. C_{sf} were used as absorbing fillers due to their unique mechanical property and suitable dielectric property, such as high strength, high modulus, low thermal expansion, and high electrical conductivity. MgO was then added to improve the mechanical properties and ensure the dielectric property of the composite simultaneously. Addition of MgO to the Al_2O_3 ceramics, the flexure strength of composite increased by 38.5% compared to pure Al_2O_3 ceramics and reached up to 270 MPa. With increasing C_{sf} content (from 0.0 to 0.5 wt%), both ε′ (from ~9 to 31.5~43) and ε″ (from ~0.0 to 16~23.6) of the C_{sf}/Al_2O_3–MgO composites increase, which is attributed to the increasing electron polarization and associated polarization relaxation, respectively.

2.8 Antibacterial Application Areas of Nanofibrous MgO Nanocomposites

Nanocomposite materials have already found commercial use across many applications such as; adsorption, catalytic process, textile products, electro devices, energy storage etc. due to their attractive properties like UV protection, flame retardancy, thermal and chemical stability, high mechanical strength and antibacterial activity [117–121]. Such properties are facilitated by the presence of the metal oxide NP such as ZnO, TiO_2, SiO_2, CuO, ZrO_2 and MgO, which positively influence antimicrobial properties [122]. However, of the available metal oxides, MgO has come to the forefront because of its various advantages that are the low-cost precursors, abundant edge/corner sites, high surface area and biocompatibility. It can also be combined with other metallic or non-metallic substances in order to enhance its biocidal and durability on substrates [123].

MgO has favourable radical formation mechanisms (singlet oxygen, hydroperoxyl, OH^- and O^{-2}) which effect antibacterial activity by causing the oxidative stress (Figure 13). Generally, the cell walls of gram-positive bacteria are more susceptible to many antimicrobial chemical/herbal compounds than gram-negative bacteria, which have more resistance owing to their lipopolysaccharides layer and periplasmic space [124]. Even so, materials could gain antibacterial property against both gram negative and gram positive bacteria after coating MgO NP [125]. NF embedded MgO (especially those with exposed [111] facets) are gaining popularity due to the integration of properties of two powerful nanomaterials and to obtain the biocompatible and antibacterial materials [125]. In the study of Dhineshbabu *et al.* [126] Nylon-6/MgO hybrid NF were produced by electrospinning and then coated on cotton fabric to investigate of antibacterial activity of the final product. The results of antibacterial tests on Staphylococcus aureus (gram positive) and Escherichia coli (gram negative) showed that use of MgO contributed to a reduction in growth of about 67% and 63% respectively. Also, addition of MgO in nylon-6 solution to produce hybrid NF supported to decrement of the viscosity and increment of the conductivity of solution which contribute to obtain homogenous and small diameter NF. Nevertheless, whilst MgO-based systems have also been shown to have antibacterial efficacy, nanofibrous outputs with such performance have not been widely reported.

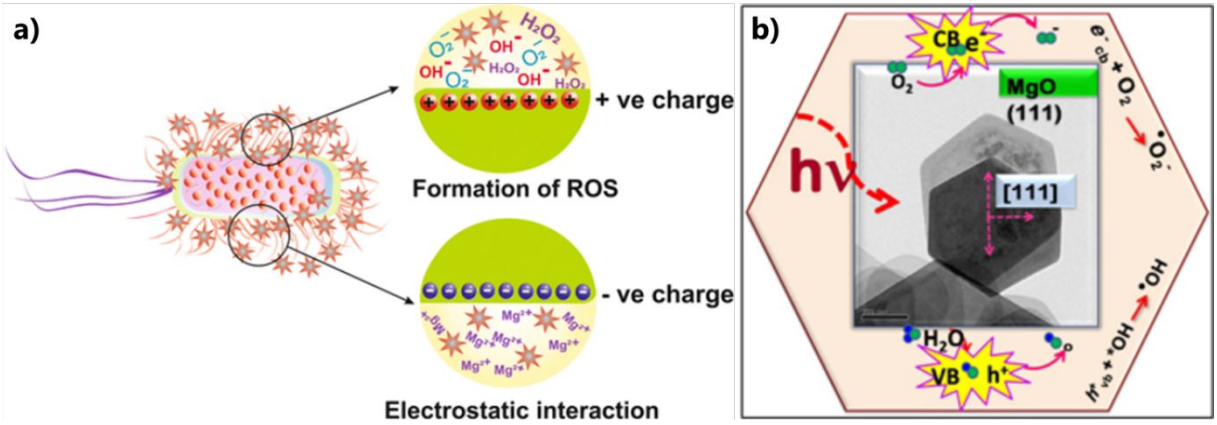

Figure 3. Graphical representation of; a) possible antibacterial mechanisms of MgO (adapted from Navik *et al*)[123], b) possible mechanisms of MgO nanoplates against *E. coli* and *B. subtilis* (adapted from Ponnuvelu *et al*)[125].

2.9 Catalytic Applications of Nanofibrous MgO Composites

The catalytic behaviour of MgO in the destructive adsorption applications and this feature have been explained in the *'Adsorption Applications of Nanofibrous MgO'* section. This section explores the applications of MgO as a catalyst-support. The function of the catalyst-supports in general is to increase the activity of the catalyst. If the catalysts are highly dispersed to the supports, the agglomeration problem of the catalysts is eliminated and no loss of activity is observed [127]. Catalyst support functionality are especially dependent on parameters such as type of metal catalyst, carbon source used and, reaction conditions to produce, for example, carbon nanotubes (CNT) and carbon nanofibers (CNF) by chemical vapor deposition (CVD) [128,129]– see Figure 14. Catalyst-supports used for such applications includes MgO, SiO_2, Al_2O_3 and TiO_2.

In a study by N. Izadi *et al.* [130] CO_2-free H_2 and CNFs have been produced over both MgO supported Ni catalyst and MgO supported bimetallic Ni (Cu, Co, Mo) catalysts via decomposition of CH_4. The catalyst components were then readily separated from CNF; MgO being more easily separated by acidic solutions, unlike other support materials such as Al_2O_3 and SiO_2 [131]. In addition, Wang and Baker[132], have used both SiO_2 and MgO as catalyst-support over Ni-Cu (4:1) catalyst for CH_4 decomposition at a reaction temperature of 725 °C and their results are shown in the Table 5.

Table 5. Effect of catalyst-support on the CH_4 conversion, lifetime and yield of H_2 and solid carbon *(adapted from Wang and Baker)*[132].

Catalyst-support	CH_4 conversion[1] (%)	Lifetime[2] (h)	Yield[3] (mol/g catalyst)	
			H_2	Carbon
Non-support	0	0	0	0
SiO_2	38.5	9	17.2	8.6
MgO	46.5	19	43.8	21.9

[1]Data obtained after 1 h. [2]Reaction had terminated when methane conversion was below 5%. [3]Yields had calculated on the basis of the weight of catalyst before reduction by Wang and Baker[132].

As seen from Table 5, the absence of the use of a catalyst-support, CH_4-conversion was not observed. Thus, it is a requirement that the support-catalyst must be used both as a dispersing agent and as a chemical component to produce H_2 and carbon via methane decomposition. MgO is seemingly a better support-catalyst, as opposed to SiO_2. This may be due to the tendency of the Ni-Cu-MgO system to form less reducible (Ni, Cu, Mg) O solid solutions during calcination. Thus, after reduction, metallic particles of smaller size are formed over MgO. Crystallite sizes of Ni-Cu alloys were also found to differ between Ni-Cu-SiO_2 and Ni-Cu-MgO catalysts (35 and 17 nm, respectively) at a reduction temperature of 600°C. Higher CNFs growth was observed in Ni-Cu-MgO catalysts because of the inverse ratio at a certain temperature between the NF growth rate and the square of particle size [132].

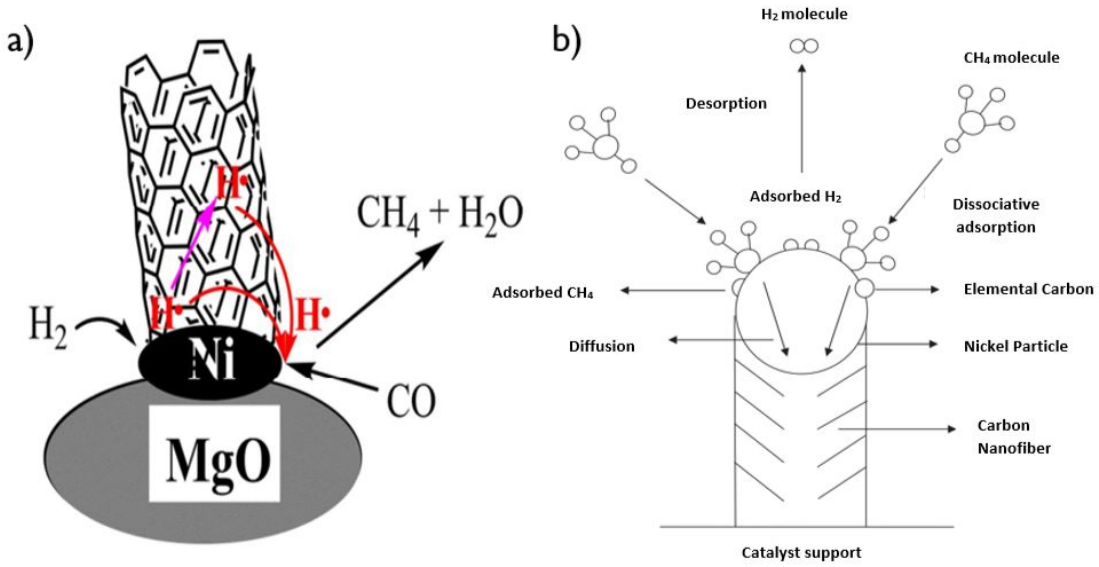

Figure 14. a) Illustration of the growth of CNTs over MgO-supported Ni catalyst *(adapted from Fan et al)*[133], b) Illustration of the growth of CNFs over MgO-supported Ni catalyst *(adapted from Izadi et al)*[130].

In the decomposition of CO over MgO-supported Ni catalysts, molecules decompose on the Ni particle surface, form carbon atoms, diffuse through the particle, and subsequently precipitate at the Ni particle/CNTs interface. The produced CNTs promoted the Ni/MgO catalyst to produce synthetic natural gas from syngas by methanation process. The smaller Ni particles provide more active sites for CO-activation and C-hydrogenation There are two CNTs properties closely related to catalytic performances for hydrogenation, one is the ability to store decomposed hydrogen on Ni, the other is the electron storage capacity, which can serve as electron channels for the catalytic reaction between CNTs and Ni particles [133].

2.10 Fire Retardant Properties of Nanofibrous MgO Composites

Owing to thermal properties (high melting point: 2850℃ and high thermal stability) of MgO [87], it can be added into NF to produce non-flammable cloths [126]. For this purpose, Venkatram *et al*. [134] produced Ag/MgO/Nylon 6 mats. On the fiber mats prepared in certain dimensions, two marks were left with a distance of 60 mm between them and the burn times between these two marks recorded for each sample. The slowest combustion rate of 1.56 mm/s was achieved using MgO (3 wt%)-$AgNO_3$ (0.25 wt%)/Nylon 6 NF. Apart from the thermal properties of MgO, it also interacts with Ag and forms a barrier that slows heat and air transfer.

Dhineshbabu *et al*. [126] investigated the flame retardancy properties of as-synthesized MgO NP/nylon-6 hybrid NF. They applied burning tests on 3 different materials, uncoated cotton (UC) fabrics, Nylon 6-coated (N6C) fabric and MgO/Nylon 6 hybrid (MgO-N6C) fabric; and demonstrated that MgO/Nylon 6 hybrid NFs (18.5 s) started burning later than uncoated cotton fabrics (6.3 s) and Nylon 6 NFs (15.4 s) (Figure 15).

Rajendran *et al*. [122] prepared a silica sol (referred to as Si) and added the MgO, ZrO_2 and TiO_2 NPs into the silica sol separately and these mixings was sonicated for 15 mins to form a composite sol (referred to as MgS, ZrS and TiS). Then, alkali treated cotton fabric samples were dipped separately into homogeneous composite-sol solutions and coated using a pad-dry cure method. They examined the contribution of metal oxide NP added to the cotton fabric for flame retardant properties and reached the results shown in Figure 15b.

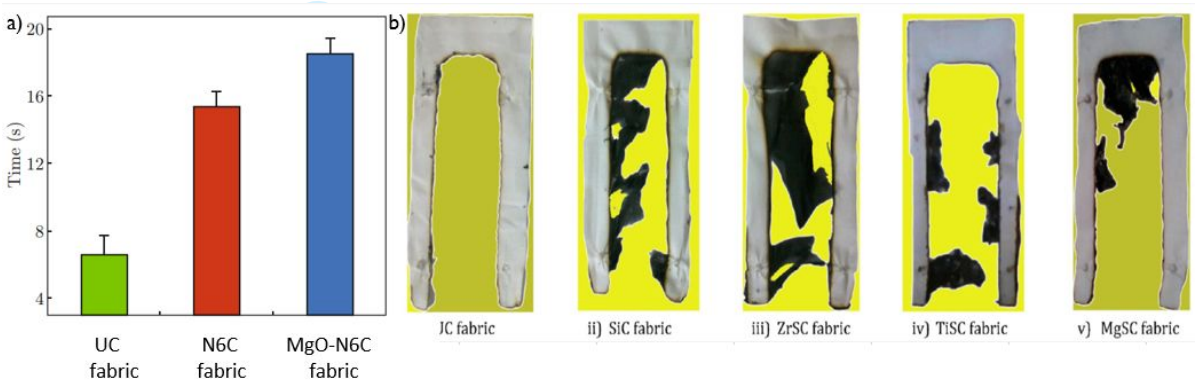

Figure 15. a) Average value of flammability of uncoated cotton (UC), Nylon 6 coated (N6C) and MgO-Nylon 6 coated (MgO-N6C) fabrics *(adapted from Dhineshbabu et al)* [126], b) Photograph image of after-burn of all coated (ZrO_2, TiO_2 and MgO) and uncoated SiC fabric samples *(adapted from Rajendran et al)* [122].

Figure 15b shows that all of the coated fabrics have unburned residues. The char formation times of nanocomposite (ZrSC, TiSC, and MgSC)-coated fabrics are 19.4, 18.9, and 18.4 seconds respectively, while SiC coated fabric forms char at 13.6s. Char formation was not observed in UC. Namely, nanocomposite coated fabrics showed higher flame retardancy than Si coated fabric and uncoated fabric [122].

2.11 Medical Applications of Nanofibrous MgO Composites

The broad medical applications of MgO-based NF span drug delivery, wound healing, tissue engineering and implant coatings [37]. Polymeric NF are of great interest in tissue engineering and wound healing, due to their ability to act as a scaffold to mimic and restore the function of tissue extracellular matrix (ECM) [20]. Such applications require a highly porous and interconnected physico-chemical fibrous structure with a large surface area that facilitates a biological environment conducive to cell attachment and proliferation as well as tissue growth and flow of nutrients. Uniform dispersion and incorporation of MgO particulates into the NF yields composite materials with enhanced structural and material properties (e.g.; tensile strength, elastic modulus, compression modulus etc.) that support effective use in biomedical applications and musculoskeletal tissue engineering.

Examples of nanofibrous architectures reported to date include MgO incorporation into; polyacrylonitrile (PAN); polycaprolactone (PCL)-chitosan (CS); and alginate-based biopolymeric non-toxic NF, as formed by electrospinning. Mechanically robust, randomly oriented alginate-based, virtually defect-free ultrafine NF (60-250 nm) were electrospun from an alginate/poly(vinyl alcohol) (PVA) polyelectrolyte complex and near-spherical MgO [24]. Tensile test to rupture revealed significant improvements in the tensile strength and elastic modulus of alginate/MgO scaffolds while retaining interfiber porosity (2–50 μm pore size), while thermal stability is improved as well. Such scaffolds have potential applications in tissue repair and regeneration as an artificial substitute for ECM.

PCL and CS-PCL composites have been the most promising, yielding dimensionally- and aqueous-stable interconnected fibrous membranes, with significantly improved mechanical properties (i.e.; tensile strength and elastic modulus) upon MgO incorporation. There is a significant decrease of fiber diameter upon incorporation of MgO (down to 0.7-1.3 μm), whilst CS-PCL/MgO based NF showed uniform surface morphology, structural integrity, and a higher Young's modulus (~25 MPa) although the ultimate tensile strength is higher for MgO-less, CS-PCL NF (~3 MPa) [20,21]. Implants for bony tissue regeneration (e.g.; to treat segmental bone defects) are critical to the success of surgery on the osteogenicity, mechanical properties and the ability of revascularization of the bioscaffold implanted. PCL/MgO composite compression modulus values (and broader mechanical properties) approach that of adult cancellous bone, meaning such materials as scaffolds may reduce the risks of adjacent level fracture, but also reinforce the non-fracture osteoporotic bone without altering the stress distribution significantly under physiological loading. PCL/MgO composites can facilitate steady, sustained release of Mg^{2+} at effective dosage for significantly enhanced local *in vivo* bone formation [135]. Subcutaneous implantation of MgO–PCL scaffolds in Sprague-Dawley rats have shown good *in vivo* biocompatibility. Favorable cell adhesion and cell attachment on these NF, via formation of hydroxyapatite layers, has been observed by numerous and long filopodia [135]. In addition, MgO seemingly offers improved cell inhibition of certain cancer cell type vs. other nanofibrous scaffolds and so, could be utilized for breast cancer therapy [27].

Despite the clear and obvious improvements that result from the incorporation of MgO in nanofibrous systems, and the impact on NF properties (e.g.; diameter, porosity, etc.), there is seemingly little interaction between the particulate MgO filler and the macromolecular polymeric host, i.e.; it is a physical interaction and mechanical dispersion [37]. Indeed, the effective synthesis of well-blended composite fibers remains a great challenge due to the lack of interaction and poor miscibility between polymers and ceramic particles at the molecular level. In cases of poor blending, this can even result in phase separation, which in turn yields poorer mechanical strength and uncontrollable material properties.

3. Conclusion and Future Outlook

This review article has focused on the various works and reports of MgO-based applications and its overlap with nanofiber-based outputs – a growing area of industrial and academic interest. A comprehensive review of the growing number of reports to date was carried out, so as to provide a unified resource for researchers going forward. As the acceptance and broader set of applications continues its exponential growth in commercial and academic output, it is

envisaged that MgO-based composites will play a central part in many future reports of nanofibrous composites (and broader composite outputs), due to the wide variety of applications to which MgO is suited, as well as other peripheral considerations such as cost, availability, ease-of-handling and use etc. Indeed, despite the many preliminary reports to date, there remains a great deal yet to discover and optimize for such systems. The authors are currently engaged in many such research efforts, especially in filtration, separation and degradation applications.

Acknowledgements

NN would like to thank TUBITAK for sponsoring a Short-term Visiting Research Fellowship to ITU, ITU TEMAG Lab. [Grant Reference Code: 21514107-115.02-E.124525, date 12.06.2018], during which time, this and other work was initiated.

REFERENCES

(1) Sridhar, R.; Venugopal, J. R.; Sundarrajan, S.; Ravichandran, R.; Ramalingam, B.; Ramakrishna, S. Electrospun Nanofibers for Pharmaceutical and Medical Applications. *J. Drug Deliv. Sci. Technol.* **2011**, *21* (6), 451–468. https://doi.org/10.1016/S1773-2247(11)50075-9.

(2) Costa, L. M. M.; de Olyveira, G. M.; Cherian, B. M.; Leão, A. L.; de Souza, S. F.; Ferreira, M. Bionanocomposites from Electrospun PVA/Pineapple Nanofibers/Stryphnodendron Adstringens Bark Extract for Medical Applications. *Ind. Crops Prod.* **2013**, *41*, 198–202. https://doi.org/10.1016/j.indcrop.2012.04.025.

(3) Elahi, Md. F.; Lu, W. Core-Shell Fibers for Biomedical Applications-A Review. *J. Bioeng. Biomed. Sci.* **2013**, *03* (01). https://doi.org/10.4172/2155-9538.1000121.

(4) Manea, L. R.; Popa, A.; Bertea, A. P. Medical Applications of Functional Electrospun Nanofibers - A Review. *Key Eng. Mater.* **2017**, *752*, 132–138. https://doi.org/10.4028/www.scientific.net/KEM.752.132.

(5) Rahman, M. M. Introductory Chapter: Overview of Nanofibers. *Nanofiber Res. - Reach. New Heights* **2016**. https://doi.org/10.5772/64370.

(6) Valipouri, A. Production Scale Up of Nanofibers: A Review. *J. Textıles Polym.* **2017**, *5* (1), 9.

(7) Burger, C.; Hsiao, B. S.; Chu, B. Nanofibrous Materials and Their Applications. *Annu. Rev. Mater. Res.* **2006**, *36* (1), 333–368. https://doi.org/10.1146/annurev.matsci.36.011205.123537.

(8) Leung, W. W.-F.; Hau, C. W.-Y.; Choy, H.-F. Microfiber-Nanofiber Composite Filter for High-Efficiency and Low Pressure Drop under Nano-Aerosol Loading. *Sep. Purif. Technol.* **2018**, *206*, 26–38. https://doi.org/10.1016/j.seppur.2018.05.033.

(9) Pei, C. C.; Kin Shing Lo, K.; Leung, W. W.-F. Titanium-Zinc-Bismuth Oxides-Graphene Composite Nanofibers as High-Performance Photocatalyst for Gas Purification. *Sep. Purif. Technol.* **2017**, *184*, 205–212. https://doi.org/10.1016/j.seppur.2017.04.016.

(10) Kenry; Lim, C. T. Nanofiber Technology: Current Status and Emerging Developments. *Prog. Polym. Sci.* **2017**, *70*, 1–17. https://doi.org/10.1016/j.progpolymsci.2017.03.002.

(11) Williams, G. R.; Raimi-Abraham, B. T.; Luo, C. J. *Nanofibres in Drug Delivery*; UCL Press, 2018. https://doi.org/10.14324/111.9781787350182.

(12) Yarin, A. L.; Koombhongse, S.; Reneker, D. H. Taylor Cone and Jetting from Liquid Droplets in Electrospinning of Nanofibers. *J. Appl. Phys.* **2001**, *90* (9), 4836–4846. https://doi.org/10.1063/1.1408260.

(13) Reneker, D. H.; Yarin, A. L. Electrospinning Jets and Polymer Nanofibers. *Polymer* **2008**, *49* (10), 2387–2425. https://doi.org/10.1016/j.polymer.2008.02.002.

(14) Barhoum, A.; Rasouli, R.; Yousefzadeh, M.; Rahier, H.; Bechelany, M. Nanofiber Technology: History and Developments. In *Handbook of Nanofibers*; Barhoum, A., Bechelany, M.,

Makhlouf, A., Eds.; Springer International Publishing: Cham, 2018; pp 1–42. https://doi.org/10.1007/978-3-319-42789-8_54-1.

(15) Romani, A. M. P. Cellular Magnesium Homeostasis. *Arch. Biochem. Biophys.* **2011**, *512* (1), 1–23. https://doi.org/10.1016/j.abb.2011.05.010.

(16) Resnick, L. M.; Gupta, R. K.; Laragh, J. H. Intracellular Free Magnesium in Erythrocytes of Essential Hypertension: Relation to Blood Pressure and Serum Divalent Cations. *Proc. Natl. Acad. Sci.* **1984**, *81* (20), 6511–6515. https://doi.org/10.1073/pnas.81.20.6511.

(17) Sharma, P.; Chung, C.; Vizcaychipi, M. Magnesium: The Neglected Electrolyte? A Clinical Review. *Pharmacol. Pharm.* **2014**, *05*, 762. https://doi.org/10.4236/pp.2014.57086.

(18) Sundarrajan, S.; Ramakrishna, S. Fabrication of Nanocomposite Membranes from Nanofibers and Nanoparticles for Protection against Chemical Warfare Stimulants. *J. Mater. Sci.* **2007**, *42* (20), 8400–8407. https://doi.org/10.1007/s10853-007-1786-4.

(19) Dadvar, S.; Tavanai, H.; Morshed, M. UV-Protection Properties of Electrospun Polyacrylonitrile Nanofibrous Mats Embedded with Mgo and Al2O3 Nanoparticles. *J. Nanoparticle Res.* **2011**, *13* (10), 5163–5169. https://doi.org/10.1007/s11051-011-0499-4.

(20) Boakye, M. A. D.; Rijal, N. P.; Adhikari, U.; Bhattarai, N. Fabrication and Characterization of Electrospun PCL-MgO-Keratin-Based Composite Nanofibers for Biomedical Applications. *Materials* **2015**, *8* (7), 4080–4095. https://doi.org/10.3390/ma8074080.

(21) Rijal, N. P.; Adhikari, U.; Khanal, S.; Pai, D.; Sankar, J.; Bhattarai, N. Magnesium Oxide-Poly(ε-Caprolactone)-Chitosan-Based Composite Nanofiber for Tissue Engineering Applications. *Mater. Sci. Eng. B* **2018**, *228*, 18–27. https://doi.org/10.1016/j.mseb.2017.11.006.

(22) Raliya, R.; Tarafdar, J. C.; Singh, S. K.; Gautam, R.; Choudhary, K.; Maurino, V. G.; Saharan, V. MgO Nanoparticles Biosynthesis and Its Effect on Chlorophyll Contents in the Leaves of Clusterbean (Cyamopsis Tetragonoloba L.). *Adv. Sci. Eng. Med. Vol. 6 Number 5 May 2014 Pp 538-5458* **2014**.

(23) Almasian, A.; Najafi, F.; Maleknia, L.; Giahi, M. Mesoporous MgO/PPG Hybrid Nanofibers: Synthesis, Optimization, Characterization and Heavy Metal Removal Property. *New J. Chem.* **2018**, *42* (3), 2013–2029. https://doi.org/10.1039/C7NJ03200E.

(24) De Silva, R. T.; Mantilaka, M. M. M. G. P. G.; Goh, K. L.; Ratnayake, S. P.; Amaratunga, G. A. J.; de Silva, K. M. N. Magnesium Oxide Nanoparticles Reinforced Electrospun Alginate-Based Nanofibrous Scaffolds with Improved Physical Properties. *Int. J. Biomater.* **2017**, *2017*, 1–9. https://doi.org/10.1155/2017/1391298.

(25) Xu, C.; Yu, Z.; Yuan, K.; Jin, X.; Shi, S.; Wang, X.; Zhu, L.; Zhang, G.; Xu, D.; Jiang, H. Improved Preparation of Electrospun MgO Ceramic Fibers with Mesoporous Structure and the Adsorption Properties for Lead and Cadmium. *Ceram. Int.* **2019**, *45* (3), 3743–3753. https://doi.org/10.1016/j.ceramint.2018.11.041.

(26) Beisenova, A.; Issatayeva, A.; Sovetov, S.; Korganbayev, S.; Jelbuldina, M.; Ashikbayeva, Z.; Blanc, W.; Schena, E.; Sales, S.; Molardi, C.; et al. Multi-Fiber Distributed Thermal Profiling of Minimally Invasive Thermal Ablation with Scattering-Level Multiplexing in MgO-Doped Fibers. *Biomed. Opt. Express* **2019**, *10* (3), 1282–1296. https://doi.org/10.1364/BOE.10.001282.

(27) Sudakaran, S. V.; Venugopal, J. R.; Vijayakumar, G. P.; Abisegapriyan, S.; Grace, A. N.; Ramakrishna, S. Sequel of MgO Nanoparticles in PLACL Nanofibers for Anti-Cancer Therapy in Synergy with Curcumin/β-Cyclodextrin. *Mater. Sci. Eng. C* **2017**, *71*, 620–628. https://doi.org/10.1016/j.msec.2016.10.050.

(28) Bakhsheshi-Rad, H. R.; Ismail, A. F.; Aziz, M.; Hadisi, Z.; Omidi, M.; Chen, X. Antibacterial Activity and Corrosion Resistance of Ta2O5 Thin Film and Electrospun PCL/MgO-Ag Nanofiber Coatings on Biodegradable Mg Alloy Implants. *Ceram. Int.* **2019**, *45* (9), 11883–11892. https://doi.org/10.1016/j.ceramint.2019.03.071.

(29) Xing, X.; Wang, Y.; Li, B. Nanofiber Drawing and Nanodevice Assembly in Poly (Trimethylene Terephthalate). *Opt. Express* **2008**, *16* (14), 10815–10822.

(30) Yoon, K.; Hsiao, B. S.; Chu, B. Functional Nanofibers for Environmental Applications. *J. Mater. Chem.* **2008**, *18* (44), 5326–5334.

(31) Hartgerink, J. D.; Beniash, E.; Stupp, S. I. Self-Assembly and Mineralization of Peptide-Amphiphile Nanofibers. *Science* **2001**, *294* (5547), 1684–1688.

(32) Ghosal, K.; Agatemor, C.; Tucker, N.; Kny, E.; Thomas, S. Electrical Spinning to Electrospinning: A Brief History. *Electrospinning* **2018**.

(33) Daristotle, J. L.; Behrens, A. M.; Sandler, A. D.; Kofinas, P. A Review of the Fundamental Principles and Applications of Solution Blow Spinning. *ACS Appl. Mater. Interfaces* **2016**, *8* (51), 34951–34963. https://doi.org/10.1021/acsami.6b12994.

(34) Zhang, X.; Lu, Y. Centrifugal Spinning: An Alternative Approach to Fabricate Nanofibers at High Speed and Low Cost. *Polym. Rev.* **2014**, *54* (4), 677–701. https://doi.org/10.1080/15583724.2014.935858.

(35) Korycka, P.; Mirek, A.; Kramek-Romanowska, K.; Grzeczkowicz, M.; Lewińska, D. Effect of Electrospinning Process Variables on The Size of Polymer Fibers and Bead-on-String Structures Established with a 23 Factorial Design. *Beilstein J. Nanotechnol.* **2018**, *9*, 2466–2478. https://doi.org/10.3762/bjnano.9.231.

(36) Pillay, V.; Dott, C.; Choonara, Y. E.; Tyagi, C.; Tomar, L.; Kumar, P.; du Toit, L. C.; Ndesendo, V. M. A Review of the Effect of Processing Variables on the Fabrication of Electrospun Nanofibers for Drug Delivery Applications. *J. Nanomater.* **2013**, *2013*.

(37) Dadvar, S.; Tavanai, H.; Morshed, M. Fabrication of Nanocomposite PAN Nanofibers Containing MgO and Al2O3 Nanoparticles. *Polym. Sci. Ser. A* **2014**, *56* (3), 358–365. https://doi.org/10.1134/S0965545X14030043.

(38) Zhu, M.; Han, J.; Wang, F.; Shao, W.; Xiong, R.; Zhang, Q.; Pan, H.; Yang, Y.; Samal, S. K.; Zhang, F.; et al. Electrospun Nanofibers Membranes for Effective Air Filtration. *Macromol. Mater. Eng.* **2017**, *302* (1), 1600353. https://doi.org/10.1002/mame.201600353.

(39) Mit-uppatham, C.; Nithitanakul, M.; Supaphol, P. Ultrafine Electrospun Polyamide-6 Fibers: Effect of Solution Conditions on Morphology and Average Fiber Diameter. *Macromol. Chem. Phys.* **2004**, *205* (17), 2327–2338. https://doi.org/10.1002/macp.200400225.

(40) Faccini, M.; Vaquero, C.; Amantia, D. Development of Protective Clothing Against Nanoparticle Based on Electrospun Nanofibers. *J Nanomater.* **2012**, *2012*, 18:1–18:9. https://doi.org/10.1155/2012/892894.

(41) Wang, Z.; Zhao, C.; Pan, Z. Porous Bead-on-String Poly(Lactic Acid) Fibrous Membranes for Air Filtration. *J. Colloid Interface Sci.* **2015**, *441*, 121–129. https://doi.org/10.1016/j.jcis.2014.11.041.

(42) Bhardwaj, N.; Kundu, S. C. Electrospinning: A Fascinating Fiber Fabrication Technique. *Biotechnol. Adv.* **2010**, *28* (3), 325–347. https://doi.org/10.1016/j.biotechadv.2010.01.004.

(43) Şener, A. G.; Altay, A. S.; Altay, F. Effect of Voltage on Morphology of Electrospun Nanofibers. In *2011 7th International Conference on Electrical and Electronics Engineering (ELECO)*; 2011; pp I-324-I–328.

(44) Givehchi, R.; Li, Q.; Tan, Z. Quality Factors of PVA Nanofibrous Filters for Airborne Particles in the Size Range of 10–125nm. *Fuel* **2016**, *181*, 1273–1280. https://doi.org/10.1016/j.fuel.2015.12.010.

(45) Choi, H. J.; Kim, S. B.; Kim, S. H.; Lee, M. H. Preparation of Electrospun Polyurethane Filter Media and Their Collection Mechanisms for Ultrafine Particles: *J. Air Waste Manag. Assoc.* **2014**.

(46) Zargham, S.; Bazgir, S.; Tavakoli, A.; Rashidi, A. S.; Damerchely, R. The Effect of Flow Rate on Morphology and Deposition Area of Electrospun Nylon 6 Nanofiber. *J. Eng. Fibers Fabr.* **2012**, *7* (4), 155892501200700400. https://doi.org/10.1177/155892501200700414.

(47) Zhang, S.; Shim, W. S.; Kim, J. Design of Ultra-Fine Nonwovens via Electrospinning of Nylon 6: Spinning Parameters and Filtration Efficiency. *Mater. Des.* **2009**, *30* (9), 3659–3666. https://doi.org/10.1016/j.matdes.2009.02.017.

(48) Aliabadi, M. Effect of Electrospinning Parameters on the Air Filtration Performance Using Electrospun Polyamide-6 Nanofibers. *Chem. Ind. Chem. Eng. Q.* **2017**, *23* (4), 441–446. https://doi.org/10.2298/CICEQ160509059A.

(49) Cheng, Y.; Wang, C.; Zhong, J.; Lin, S.; Xiao, Y.; Zhong, Q.; Hulin, J.; Nan, W.; Wenbo, L.; Shuwen, C.; et al. Electrospun Polyetherimide Electret Nonwoven for Bi-Functional Smart Face Mask. *Nano Energy* **2017**, 34: 562-569.

(50) De Vrieze, S.; Van Camp, T.; Nelvig, A.; Hagström, B.; Westbroek, P.; De Clerck, K. The Effect of Temperature and Humidity on Electrospinning. *J. Mater. Sci.* **2009**, *44* (5), 1357–1362. https://doi.org/10.1007/s10853-008-3010-6.

(51) Casper, C. L.; Stephens, J. S.; Tassi, N. G.; Chase, D. B.; Rabolt, J. F. Controlling Surface Morphology of Electrospun Polystyrene Fibers: Effect of Humidity and Molecular Weight in the Electrospinning Process. *Macromolecules* **2004**, *37* (2), 573–578. https://doi.org/10.1021/ma0351975.

(52) Pimentel, D.; Cooperstein, S.; Randell, H.; Filiberto, D.; Sorrentino, S.; Kaye, B.; Nicklin, C.; Yagi, J.; Brian, J.; O'Hern, J.; et al. Ecology of Increasing Diseases: Population Growth and Environmental Degradation. *Hum. Ecol.* **2007**, *35* (6), 653–668. https://doi.org/10.1007/s10745-007-9128-3.

(53) Cornell University. Pollution Causes 40 Percent of Deaths Worldwide, Study Finds https://www.sciencedaily.com/releases/2007/08/070813162438.htm (accessed Feb 17, 2019).

(54) US EPA, O. Technical Overview of Volatile Organic Compounds https://www.epa.gov/indoor-air-quality-iaq/technical-overview-volatile-organic-compounds (accessed May 15, 2019).

(55) Khan, F. I.; Kr. Ghoshal, A. Removal of Volatile Organic Compounds from Polluted Air. *J. Loss Prev. Process Ind.* **2000**, *13* (6), 527–545. https://doi.org/10.1016/S0950-4230(00)00007-3.

(56) Barea, E.; Montoro, C.; Navarro, J. A. R. Toxic Gas Removal – Metal–Organic Frameworks for the Capture and Degradation of Toxic Gases and Vapours. *Chem Soc Rev* **2014**, *43* (16), 5419–5430. https://doi.org/10.1039/C3CS60475F.

(57) Brown, S. K.; Sim, M. R.; Abramson, M. J.; Gray, C. N. Concentrations of Volatile Organic Compounds in Indoor Air – A Review. *Indoor Air* **1994**, *4* (2), 123–134. https://doi.org/10.1111/j.1600-0668.1994.t01-2-00007.x.

(58) Kadam, V. V.; Wang, L.; Padhye, R. Electrospun Nanofibre Materials to Filter Air Pollutants – A Review. *J. Ind. Text. 2018 478 2253-2280* **2018**.

(59) Kim, J. M.; Kim, J. H.; Lee, C. Y.; Jerng, D. W.; Ahn, H. S. Toluene and Acetaldehyde Removal from Air on to Graphene-Based Adsorbents with Microsized Pores. *J. Hazard. Mater.* **2018**, *344*, 458–465. https://doi.org/10.1016/j.jhazmat.2017.10.038.

(60) Li, L.; Sun, Z.; Li, H.; Keener, T. C. Effects of Activated Carbon Surface Properties on the Adsorption of Volatile Organic Compounds. *J. Air Waste Manag. Assoc.* **2012**, *62* (10), 1196–1202. https://doi.org/10.1080/10962247.2012.700633.

(61) Zhang, X.; Gao, B.; Creamer, A. E.; Cao, C.; Li, Y. Adsorption of VOCs onto Engineered Carbon Materials: A Review. *J. Hazard. Mater.* **2017**, *338*, 102–123. https://doi.org/10.1016/j.jhazmat.2017.05.013.

(62) Wang, S.-X.; Yap, C. C.; He, J.; Chen, C.; Wong, S. Y.; Li, X. Electrospinning: A Facile Technique for Fabricating Functional Nanofibers for Environmental Applications : Nanotechnology Reviews https://www.degruyter.com/view/j/ntrev.2016.5.issue-1/ntrev-2015-0065/ntrev-2015-0065.xml (accessed May 15, 2019). https://doi.org/10.1515/ntrev-2015-0065.

(63) Sharma, N.; Kakkar, R. Recent Advancements on Warfare Agents/Metal Oxides Surface Chemistry and Their Simulation Study. *Adv. Mater. Lett.* **2013**, *4* (7), 508–521. https://doi.org/10.5185/amlett.2012.12493.

(64) Nazari, B.; Jaafari, M. A New Method for the Synthesis of MgO Nanoparticles for the Destructive Adsorption of Organo-Phosphorus Compounds. *Dig. J. Nanomater. Biostructures DJNB* **2010**, 10.

(65) Li, Y. X.; Koper, O.; Atteya, M.; Klabunde, K. J. Adsorption and Decomposition of Organophosphorus Compounds on Nanoscale Metal Oxide Particles. In Situ GC-MS Studies of Pulsed Microreactions over Magnesium Oxide. *Chem. Mater.* **1992**, *4* (2), 323–330. https://doi.org/10.1021/cm00020a019.

(66) Sundarrajan, S.; Chandrasekaran, A. R.; Ramakrishna, S. An Update on Nanomaterials-Based Textiles for Protection and Decontamination: An Update on Nanomaterials-Based Textiles. *J. Am. Ceram. Soc.* **2010**, *93* (12), 3955–3975. https://doi.org/10.1111/j.1551-2916.2010.04117.x.

(67) Li, D.; Xia, Y. Electrospinning of Nanofibers: Reinventing the Wheel? *Adv. Mater.* **2004**, *16* (14), 1151–1170. https://doi.org/10.1002/adma.200400719.

(68) Michalkova, A.; Ilchenko, M.; Gorb, L.; Leszczynski, J. Theoretical Study of the Adsorption and Decomposition of Sarin on Magnesium Oxide. *J. Phys. Chem. B* **2004**, *108* (17), 5294–5303. https://doi.org/10.1021/jp036766d.

(69) Branda, M. M.; Rodríguez, A. H.; Belelli, P. G.; Castellani, N. J. Ethanol Adsorption on MgO Surface with and without Defects from a Theoretical Point of View. *Surf. Sci.* **2009**, *603* (8), 1093–1098. https://doi.org/10.1016/j.susc.2009.02.021.

(70) Dadvar, S.; Tavanai, H.; Morshed, M. Effect of Embedding MgO and Al2O3 Nanoparticles in the Precursor on the Pore Characteristics of PAN Based Activated Carbon Nanofibers. *J. Anal. Appl. Pyrolysis* **2012**, *98*, 98–105. https://doi.org/10.1016/j.jaap.2012.08.001.

(71) Branda, M.; Ferullo, R. M.; Belelli, P. G.; Castellani, N. Methanol Adsorption on Magnesium Oxide Surface with Defects: A DFT Study. *Surf. Sci.* **2003**, *527*, 89–99. https://doi.org/10.1016/S0039-6028(03)00010-4.

(72) Dadvar, S.; Tavanai, H.; Morshed, M.; Ghiaci, M. A Study on the Kinetics of 2-Chloroethyl Ethyl Sulfide Adsorption onto Nanocomposite Activated Carbon Nanofibers Containing Metal Oxide Nanoparticles. *Sep. Purif. Technol.* **2013**, *114*, 24–30. https://doi.org/10.1016/j.seppur.2013.04.019.

(73) Dadvar, S.; Tavanai, H.; Morshed, M.; Ghiaci, M. The Removal of 2-Chloroethyl Ethyl Sulfide Using Activated Carbon Nanofibers Embedded with MgO and Al_2O_3 Nanoparticles. *J. Chem. Eng. Data* **2012**, *57* (5), 1456–1462. https://doi.org/10.1021/je201328s.

(74) Behnam, R.; Morshed, M.; Tavanai, H.; Ghiaci, M. Destructive Adsorption of Diazinon Pesticide by Activated Carbon Nanofibers Containing Al2O3 and MgO Nanoparticles. *Bull. Environ. Contam. Toxicol.* **2013**, *91* (4), 475–480. https://doi.org/10.1007/s00128-013-1064-x.

(75) Lange, L. E.; Obendorf, S. K. Effect of Plasma Etching on Destructive Adsorption Properties of Polypropylene Fibers Containing Magnesium Oxide Nanoparticles. *Arch. Environ. Contam. Toxicol.* **2012**, *62* (2), 185–194. https://doi.org/10.1007/s00244-011-9702-y.

(76) Che Othman, F. E.; Yusof, N.; Hasbullah, H.; Jaafar, J.; Ismail, A. F.; Abdullah, N.; Md Nordin, N. A. H.; Aziz, F.; Wan Salleh, W. N. Polyacrylonitrile/Magnesium Oxide-Based Activated Carbon Nanofibers with Well-Developed Microporous Structure and Their Adsorption Performance for Methane. *J. Ind. Eng. Chem.* **2017**, *51*, 281–287. https://doi.org/10.1016/j.jiec.2017.03.014.

(77) Yusof, N. Adsorption of Cadmium (Ii) Ions by Polyacrylonitrile-Based Activated Carbon Nanofibers/Magnesium Oxide as Its Adsorbents. *Malays. J. Anal. Sci.* **2016**, *20* (6), 1467–1473. https://doi.org/10.17576/mjas-2016-2006-27.

(78) Hussain, M. M.; Guven, N.; Rankumar, S. Self Cleaning Nanofiber Webs.

(79) Ren, B. Electrospinning Synthesis of MgO Nanofibers and Properties of Uranium (VI)-Sorption. *J Chem Soc Pak 2014 362 250-254* 5.

(80) Zhang, Y.-L.; Cao, F. Fine Particulate Matter ($PM_{2.5}$) in China at a City Level. *Sci. Rep.* **2015**, *5*, 14884. https://doi.org/10.1038/srep14884.

(81) Xing, Y.-F.; Xu, Y.-H.; Shi, M.-H.; Lian, Y.-X. The Impact of PM2.5 on the Human Respiratory System. *J. Thorac. Dis.* **2016**, *8* (1), E69–E74. https://doi.org/10.3978/j.issn.2072-1439.2016.01.19.

(82) Choi, H.-J.; Kumita, M.; Hayashi, S.; Yuasa, H.; Kamiyama, M.; Seto, T.; Tsai, C.-J.; Otani, Y. Filtration Properties of Nanofiber/Microfiber Mixed Filter and Prediction of Its Performance. *Aerosol Air Qual. Res.* **2017**, *17* (4), 1052–1062. https://doi.org/10.4209/aaqr.2016.06.0256.

(83) Farizatto, K. L. G.; Bahr, B. A. Paraoxon: An Anticholinesterase That Triggers an Excitotoxic Cascade of Oxidative Stress, Adhesion Responses, and Synaptic Compromise. *Eur. Sci. J. ESJ* **2017**, *13* (10). https://doi.org/10.19044/esj.2017.v13n10p%p.

(84) Wei, X.; Li, C.; Wang, C.; Lin, S.; Wu, J.; Guo, M. Rapid and Destructive Adsorption of Paraoxon-Ethyl Toxin via a Self-Detoxifying Hybrid Electrospun Nanofibrous Membrane. *Chem. Eng. J.* **2018**, *351*, 31–39. https://doi.org/10.1016/j.cej.2018.06.090.

(85) Sellik, A.; Pollet, T.; Ouvry, L.; Briançon, S.; Fessi, H.; Hartmann, D. J.; Renaud, F. N. R. Degradation of Paraoxon (VX Chemical Agent Simulant) and Bacteria by Magnesium Oxide Depends on the Crystalline Structure of Magnesium Oxide. *Chem. Biol. Interact.* **2017**, *267*, 67–73. https://doi.org/10.1016/j.cbi.2016.11.023.

(86) Dehghan, S. F.; Golbabaei, F.; Maddah, B.; Latifi, M.; Pezeshk, H.; Hasanzadeh, M.; Akbar-Khanzadeh, F. Optimization of Electrospinning Parameters for Polyacrylonitrile-MgO Nanofibers Applied in Air Filtration. *J. Air Waste Manag. Assoc.* **2016**, *66* (9), 912–921. https://doi.org/10.1080/10962247.2016.1162228.

(87) Metals, A. S. for. *Fiber-Strengthened Metallic Composites*; ASTM International, 1967.

(88) Lin, X.; Liu, B.; Wang, X.; Zhu, L.; Jin, X.; Liu, X.; Zhang, G.; Xu, D. Large Scale Fabrication Of Magnesium Oxide Fibers For High Temperature Thermal Structure Applications. *Ceram. Int.* **2017**, *43* (1), 1455–1459. https://doi.org/10.1016/j.ceramint.2016.10.113.

(89) Xie, Y.; Sherwood, P. M. A. Coatings of Aluminum Oxide and Magnesium Oxide on Carbon Fiber Surfaces. *Chem. Mater.* **1994**, *6* (5), 650–657. https://doi.org/10.1021/cm00041a016.

(90) De Silva, R. T.; Mantilaka, M. M. M. G. P. G.; Ratnayake, S. P.; Amaratunga, G. A. J.; de Silva, K. M. N. Nano-MgO Reinforced Chitosan Nanocomposites for High Performance Packaging Applications with Improved Mechanical, Thermal and Barrier Properties. *Carbohydr. Polym.* **2017**, *157*, 739–747. https://doi.org/10.1016/j.carbpol.2016.10.038.

(91) Swaroop, C.; Shukla, M. Nano-Magnesium Oxide Reinforced Polylactic Acid Biofilms for Food Packaging Applications. *Int. J. Biol. Macromol.* **2018**, *113*, 729–736. https://doi.org/10.1016/j.ijbiomac.2018.02.156.

(92) Sanuja, S.; Agalya, A.; Umapathy, M. J. Studies on Magnesium Oxide Reinforced Chitosan Bionanocomposite Incorporated with Clove Oil for Active Food Packaging Application. *Int. J. Polym. Mater. Polym. Biomater.* **2014**, *63* (14), 733–740. https://doi.org/10.1080/00914037.2013.879445.

(93) Almerindo, G. I.; Probst, L. F. D.; Campos, C. E. M.; de Almeida, R. M.; Meneghetti, S. M. P.; Meneghetti, M. R.; Clacens, J.-M.; Fajardo, H. V. Magnesium Oxide Prepared via Metal–Chitosan Complexation Method: Application as Catalyst for Transesterification of Soybean Oil and Catalyst Deactivation Studies. *J. Power Sources* **2011**, *196* (19), 8057–8063. https://doi.org/10.1016/j.jpowsour.2011.05.030.

(94) Gupta, A.; Avcı, P.; Dai, T.; Huang, Y. Y.; Hamblin, M. R. Ultraviolet Radiation in Wound Care: Sterilization and Stimulation | Advances in Wound Care. *Adv. Wound Care 2013 28 422-437*.

(95) Ohnaka, T. [Health effects of ultraviolet radiation]. *Ann. Physiol. Anthropol. Seiri Jinruigaku Kenkyukai Kaishi* **1993**, *12* (1), 1–10.

(96) Wong, W.; Lam, J. K.-C.; Kan, C.; Postle, R. Influence of Knitted Fabric Construction on the Ultraviolet Protection Factor of Greige and Bleached Cotton Fabrics. *Text. Res. J.* **2013**, *83* (7), 683–699.

(97) Wong, W. Y.; Lam, J. K. C.; Kan, C. W.; Postle, R. In Vitro Assessment of Ultraviolet Protection of Coloured Cotton Knitted Fabrics with Different Structures under Stretched and Wet Conditions. *Radiat. Prot. Dosimetry* **2014**, *164* (3), 325–334.

(98) Li, X.; Yuan, Y.; Zhang, J.; Kim, T.; Zhang, D.; Yang, K.; Lee, Y.; Wang, L. Pressure-Induced Photoluminescence of MgO. *J. Phys. Condens. Matter* **2018**, *30* (19), 194002. https://doi.org/10.1088/1361-648X/aabb40.

(99) Janet, C. M.; Viswanathan, B.; Viswanath, R. P.; Varadarajan, T. K. Characterization and Photoluminescence Properties of MgO Microtubes Synthesized from Hydromagnesite Flowers. *J. Phys. Chem. C* **2007**, *111* (28), 10267–10272. https://doi.org/10.1021/jp072539q.

(100) Bos, A. J. J.; Prokić, M.; Brouwer, J. C. Optically and Thermally Stimulated Luminescence Characteristics of MgO:Tb3+. *Radiat. Prot. Dosimetry* **2006**, *119* (1–4), 130–133. https://doi.org/10.1093/rpd/nci641.

(101) Kafizas, A.; Wang, X.; Pendlebury, S. R.; Barnes, P.; Ling, M.; Sotelo-Vazquez, C.; Quesada-Cabrera, R.; Li, C.; Parkin, I. P.; Durrant, J. R. Where Do Photogenerated Holes Go in Anatase:Rutile TiO2? A Transient Absorption Spectroscopy Study of Charge Transfer and Lifetime. *J. Phys. Chem. A* **2016**, *120* (5), 715–723. https://doi.org/10.1021/acs.jpca.5b11567.

(102) Moniz, S. J. A.; Shevlin, S. A.; Martin, D. J.; Guo, Z.-X.; Tang, J. Visible-Light Driven Heterojunction Photocatalysts for Water Splitting – a Critical Review. *Energy Environ. Sci.* **2015**, *8* (3), 731–759. https://doi.org/10.1039/C4EE03271C.

(103) Sachs, M.; Park, J.-S.; Pastor, E.; Kafizas, A.; A. Wilson, A.; Francàs, L.; Gul, S.; Ling, M.; Blackman, C.; Yano, J.; et al. Effect of Oxygen Deficiency on the Excited State Kinetics of WO 3 and Implications for Photocatalysis. *Chem. Sci.* **2019**, *10* (22), 5667–5677. https://doi.org/10.1039/C9SC00693A.

(104) Mantilaka, M. M. M. G. P. G.; De Silva, R. T.; Ratnayake, S. P.; Amaratunga, G.; de Silva, K. M. N. Photocatalytic Activity of Electrospun MgO Nanofibres: Synthesis, Characterization and Applications. *Mater. Res. Bull.* **2018**, *99*, 204–210. https://doi.org/10.1016/j.materresbull.2017.10.047.

(105) Sharma, S. K. *Green Chemistry for Dyes Removal from Waste Water: Research Trends and Applications*; John Wiley & Sons, 2015.

(106) Li, X. Z.; Zhao, Y. G. Advanced Treatment of Dyeing Wastewater for Reuse. *Water Sci. Technol.* **1999**, *39* (10–11), 249–255. https://doi.org/10.2166/wst.1999.0664.

(107) Roy, D. C.; Biswas, S. K.; Saha, A. K.; Sikdar, B.; Rahman, M.; Roy, A. K.; Prodhan, Z. H.; Tang, S.-S. Biodegradation of Crystal Violet Dye by Bacteria Isolated from Textile Industry Effluents. *PeerJ* **2018**, *6*, e5015. https://doi.org/10.7717/peerj.5015.

(108) Abidin, C. Z. A.; Ong, S. A.; Makhtar, S. N. N.; Rahmat, N. R.; Ahmad, R. Decolourization and Cod Reduction of Textile Wastewater by Ozonation in Combination with Biological Treatment. *Int. J. Automot. Mech. Eng.* **2016**, *13* (1).

(109) Mohammed, M. A.; Shitu, A.; Abdullah, A. Removal of Methylene Blue Using Low Cost Adsorbent: A Review. *Res. J. Chem. Sci. ISSN 2014 2231 606X*.

(110) Zheng, Y.; Cao, L.; Xing, G.; Bai, Z.; Huang, J.; Zhang, Z. Microscale Flower-like Magnesium Oxide for Highly Efficient Photocatalytic Degradation of Organic Dyes in Aqueous Solution. *RSC Adv.* **2019**, *9* (13), 7338–7348. https://doi.org/10.1039/C8RA10385B.

(111) Hornak, J.; Trnka, P.; Kadlec, P.; Michal, O.; Mentlík, V.; Šutta, P.; Csányi, G.; Tamus, Z. Magnesium Oxide Nanoparticles: Dielectric Properties, Surface Functionalization and Improvement of Epoxy-Based Composites Insulating Properties. *Nanomaterials* **2018**, *8* (6), 381. https://doi.org/10.3390/nano8060381.

(112) Youssef, M.; Van Vliet, K. J.; Yildiz, B. Polarizing Oxygen Vacancies in Insulating Metal Oxides under a High Electric Field. *Phys. Rev. Lett.* **2017**, *119* (12), 126002. https://doi.org/10.1103/PhysRevLett.119.126002.

(113) Sun, W.; Sun, X.; Peng, Q.; Wang, H.; Ge, Y.; Akhtar, N.; Huang, Y.; Wang, K. Nano-MgO/AB Decorated Separator to Suppress Shuttle Effect of Lithium–Sulfur Battery. *Nanoscale Adv.* **2019**, *1* (4), 1589–1597. https://doi.org/10.1039/C8NA00420J.

(114) Ahmad, Z. Polymer Dielectric Materials. *Dielectr. Mater.* **2012**. https://doi.org/10.5772/50638.

(115) Pattanshetti, V. V.; Shashidhara, G. M.; Veena, M. G. Dielectric and Thermal Properties of Magnesium Oxide/Poly(Aryl Ether Ketone) Nanocomposites. *Sci. Eng. Compos. Mater.* **2018**, *25* (5), 915–925. https://doi.org/10.1515/secm-2016-0273.

(116) Huang, S.; Zhou, W.; Luo, F.; Wei, P.; Zhu, D. Mechanical and Dielectric Properties of Short Carbon Fiber Reinforced Al2O3 Composites with MgO Additive. *Ceram. Int.* **2014**, *40* (2), 2785–2791. https://doi.org/10.1016/j.ceramint.2013.10.038.

(117) Mishra, A. K.; Valodkar, M. C. Polymer Nanocomposites for Energy and Fuel Cell Applications. In *Properties and Applications of Polymer Nanocomposites: Clay and Carbon Based Polymer Nanocomposites*; Tripathy, D. K., Sahoo, B. P., Eds.; Springer Berlin Heidelberg: Berlin, Heidelberg, 2017; pp 107–137. https://doi.org/10.1007/978-3-662-53517-2_6.

(118) Pramanik, S.; Karak, N. Polymer Nanocomposites for Adhesive, Coating, and Paint Applications. In *Properties and Applications of Polymer Nanocomposites: Clay and Carbon Based Polymer Nanocomposites*; Tripathy, D. K., Sahoo, B. P., Eds.; Springer Berlin Heidelberg: Berlin, Heidelberg, 2017; pp 173–204. https://doi.org/10.1007/978-3-662-53517-2_8.

(119) Sahoo, B. P.; Tripathy, D. K. Polymer Nanocomposites for Electronics, Dielectrics, and Microwave Applications. In *Properties and applications of polymer nanocomposites: clay and carbon-based polymer nanocomposites*; Tripathy, D. K., Sahoo, B. P., Eds.; Springer Berlin Heidelberg: Berlin, Heidelberg, 2017; pp 25–36. https://doi.org/10.1007/978-3-662-53517-2_2.

(120) Sahoo, T. R. Polymer Nanocomposites for Environmental Applications. In *Properties and Applications of Polymer Nanocomposites: Clay and Carbon Based Polymer Nanocomposites*; Tripathy, D. K., Sahoo, B. P., Eds.; Springer Berlin Heidelberg: Berlin, Heidelberg, 2017; pp 77–106. https://doi.org/10.1007/978-3-662-53517-2_5.

(121) Tripathy, J. Polymer Nanocomposites for Biomedical and Biotechnology Applications. In *Properties and applications of polymer nanocomposites: clay and carbon-based polymer nanocomposites*; Tripathy, D. K., Sahoo, B. P., Eds.; Springer Berlin Heidelberg: Berlin, Heidelberg, 2017; pp 57–76. https://doi.org/10.1007/978-3-662-53517-2_4.

(122) Rajendran, V.; Dhineshbabu, N. R.; Kanna, R. R.; Kaler, K. V. I. S. Enhancement of Thermal Stability, Flame Retardancy, and Antimicrobial Properties of Cotton Fabrics Functionalized by Inorganic Nanocomposites. *Ind. Eng. Chem. Res.* **2014**, *53* (50), 19512–19524. https://doi.org/10.1021/ie502584m.

(123) Navik, R.; Thirugnanasampanthan, L.; Venkatesan, H.; Kamruzzaman, Md.; Shafiq, F.; Cai, Y. Synthesis and Application of Magnesium Peroxide on Cotton Fabric for Antibacterial Properties. *Cellulose* **2017**, *24* (8), 3573–3587. https://doi.org/10.1007/s10570-017-1356-0.

(124) Koohsari, H.; Ghaemi, E.; Sadegh Sheshpoli, M.; Jahedi, M.; Zahiri, M. The Investigation of Antibacterial Activity of Selected Native Plants from North of Iran. *J. Med. Life* **2015**, *8* (Spec Iss 2), 38–42.

(125) Ponnuvelu, D. V.; Selvaraj, A.; Suriyaraj, S. P.; Selvakumar, R.; Pulithadathail, B. Ultrathin Hexagonal MgO Nanoflakes Coated Medical Textiles and Their Enhanced Antibacterial Activity. *Mater. Res. Express* **2016**, *3* (10), 105005. https://doi.org/10.1088/2053-1591/3/10/105005.

(126) Dhineshbabu, N. R.; Karunakaran, G.; Suriyaprabha, R.; Manivasakan, P.; Rajendran, V. Electrospun MgO/Nylon 6 Hybrid Nanofibers for Protective Clothing. *Nano-Micro Lett.* **2014**, *6* (1). https://doi.org/10.5101/nml.v6i1.p46-54.

(127) Zhang, Y.; Tang, Y. H.; Zhang, E. L.; Lin, L. W.; Pei, L. Z. Preparation of Ni/MgO Catalysts for Carbon Nanofibres by a Self-Propagating Low Temperature Combustion Process. *Mater Sci-Pol. 2010 28 805-815* 11.

(128) Wang, Y.; Shah, N.; Huffman, G. P. Simultaneous Production of Hydrogen and Carbon Nanostructures by Decomposition of Propane and Cyclohexane over Alumina Supported Binary Catalysts. *Catal. Today* **2005**, *99* (3), 359–364. https://doi.org/10.1016/j.cattod.2004.10.012.

(129) Shen, W.; Huggins, F. E.; Shah, N.; Jacobs, G.; Wang, Y.; Shi, X.; Huffman, G. P. Novel Fe–Ni Nanoparticle Catalyst for the Production of CO- and CO2-Free H2 and Carbon Nanotubes by

Dehydrogenation of Methane. *Appl. Catal. Gen.* **2008**, *351* (1), 102–110. https://doi.org/10.1016/j.apcata.2008.09.004.

(130) Izadi, N.; Rashidi, A.; Borghei, M.; Karimzadeh, R.; Tofigh, A. Synthesis of Carbon Nanofibres over Nanoporous Ni–MgO Catalyst: Influence of the Bimetallic Ni–(Cu, Co, Mo) MgO Catalysts. *J. Exp. Nanosci.* **2012**, *7* (2), 160–173. https://doi.org/10.1080/17458080.2010.513019.

(131) Zheng, G.-B.; Kouda, K.; Sano, H.; Uchiyama, Y.; Shi, Y.-F.; Quan, H.-J. A Model for the Structure and Growth of Carbon Nanofibers Synthesized by the CVD Method Using Nickel as a Catalyst. *Carbon* **2004**, *42* (3), 635–640. https://doi.org/10.1016/j.carbon.2003.12.077.

(132) Wang, H.; Baker, R. T. K. Decomposition of Methane over a Ni−Cu−MgO Catalyst to Produce Hydrogen and Carbon Nanofibers. *J. Phys. Chem. B* **2004**, *108* (52), 20273–20277. https://doi.org/10.1021/jp040496x.

(133) Fan, M. T.; Lin, J. D.; Zhang, H. B.; Liao, D. W. In-Situ Growth of Carbon Nanotubes on Ni/MgO: A Facile Preparation of Efficient Catalysts for the Production of Synthetic Natural Gas from Syngas. *Chem. Commun. 2015 5186 15720-15723* 5.

(134) Venkatram, M.; Narasimha Murthy, H. N. R.; Gaikwad, A.; Mankunipoyil, S. A.; Ramakrishna, S.; Ayalasomayajula Ratna, P. Antibacterial and Flame-Retardant Properties of Ag-MgO/Nylon 6 Electrospun Nanofibers for Protective Applications. *Cloth. Text. Res. J.* **2018**, *36* (4), 296–309. https://doi.org/10.1177/0887302X18783071.

(135) Suryavanshi, A.; Khanna, K.; Sindhu, K. R.; Bellare, J.; Srivastava, R. Magnesium Oxide Nanoparticle-Loaded Polycaprolactone Composite Electrospun Fiber Scaffolds for Bone–Soft Tissue Engineering Applications: *In-Vitro* and *in-Vivo* Evaluation. *Biomed. Mater.* **2017**, *12* (5), 055011. https://doi.org/10.1088/1748-605X/aa792b.

Nanofibrous MgO Composites: Structures, Properties and Applications

Tuğba Baysal[1,2], Nuruzzaman Noor[3], Ali Demir[4]

[1]MSc Student at Istanbul Technical University, Nanoscience and Nanoengineering Programme, Istanbul-Turkey

[2]Research Assistant at Burdur Mehmet Akif Ersoy University, Department of Nanoscience and Nanotechnology, Burdur-Turkey

[3]Research Assistant Professor at The Hong Kong Polytechnic University, Institute of Textiles and Clothing, Hong Kong

[4]Prof. Dr. at Istanbul Technical University, Department of Textile Engineering, Istanbul-Turkey

(Corresponding Author: ademir@itu.edu.tr)

GRAPHICAL ABSTRACT

Nanomaterials have become an established area of academic research and they have gained commercial importance due to their valuable physico-chemical properties, such as large surface area, high mechanical strength as well as unique optical and electrical features. Numerous nanosize architectures have been researched and reported to date including quantum dots, fullerenes, nanorods, nanowires, nanofibers, nanosheets, nanowalls, nanocoils and nanoballs etc. Among these materials, nanofibers are extremely valuable morphologies used across many industries spanning from textile to medical applications and beyond. This review article has focused on the various works and reports of MgO-based applications and its overlap with nanofiber-based structures – a growing area of industrial and academic interest. A comprehensive review of the growing number of reports to date was carried out, so as to provide a unified resource for researchers going forward. As the acceptance and broader set of applications continues its exponential growth in commercial and academic output, it is envisaged that MgO-based composites will play a central part in many future reports of nanofibrous composites (and broader composite), due to the wide variety of applications to which MgO is suited, as well as other peripheral properties such as cost, availability, ease-of-handling and use etc. Indeed, despite the many preliminary reports to date, there remains a great deal yet to discover and optimise for such systems.

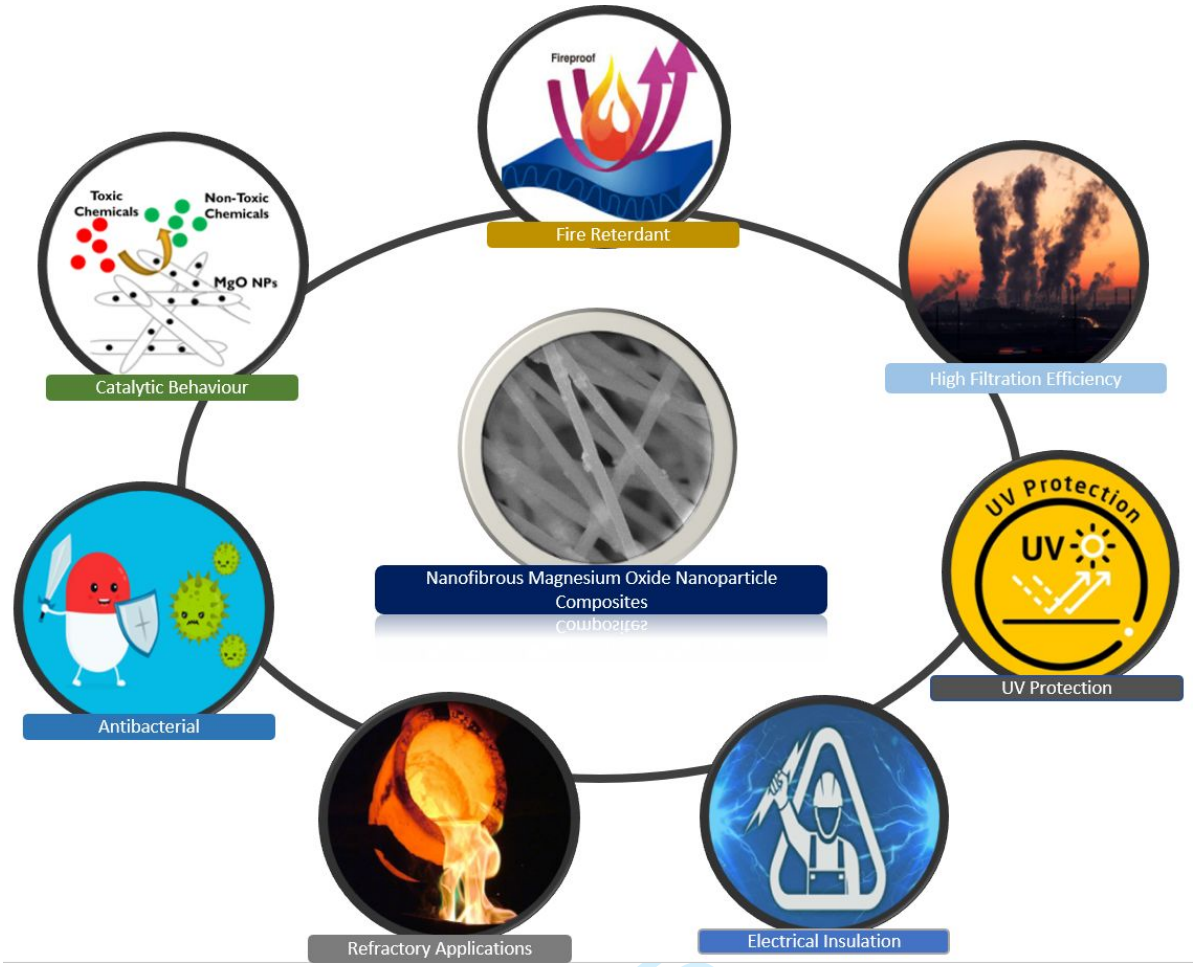

Figure 2. Illustrative overview of the broad number of potential applications of nanofibrous MgO nanoparticle composites

.

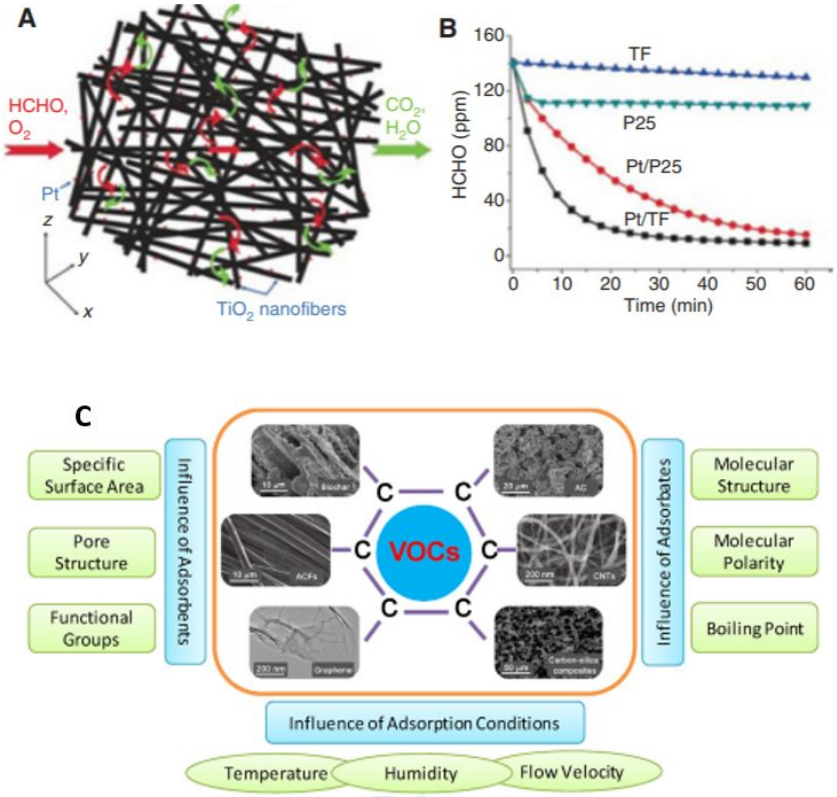

Figure 3. A) Illustration of the fast diffusion of reactants (HCHO and O_2) and products (CO_2 and H_2O) in the hierarchically porous channel of the Pt/TF catalyst *(adapted from Wang et al)* [62], B) Changes in formaldehyde (HCHO) concentration as a function of reaction time for the Pt/P25 and Pt/TF samples *(adapted from Wang et al)* [62], C) The important parameters of VOCs adsorption *(adapted from Zhang et al)*[61].

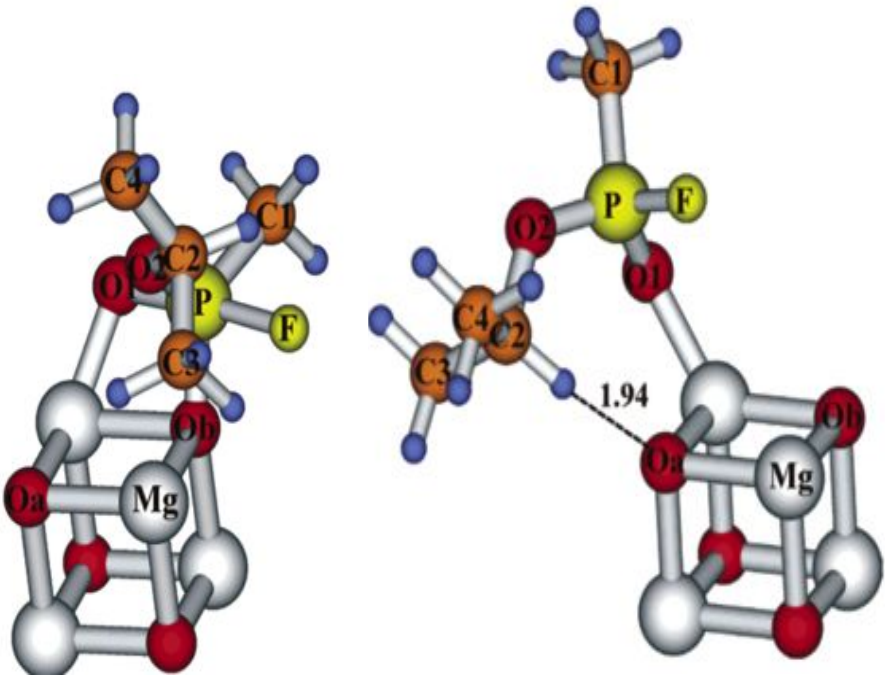

Figure 4. Schematic representation of the geometric structure of magnesium oxide (Mg_4O_4)-Sarin adsorbed system (*adapted from Michalkova et al*) [68].

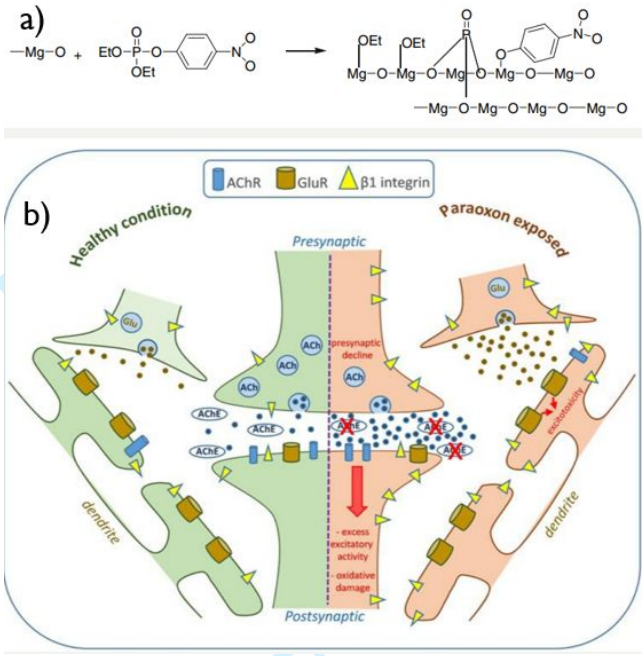

Figure 6. a) Decomposition mechanism of paraoxon on MgO surface (*adapted from Sundarrajan and Ramakrishna*)[18] b) Schematic representation of paraoxon-induced cell disorders in brain tissue (*adapted from Farizatto and Bahr*)[83].

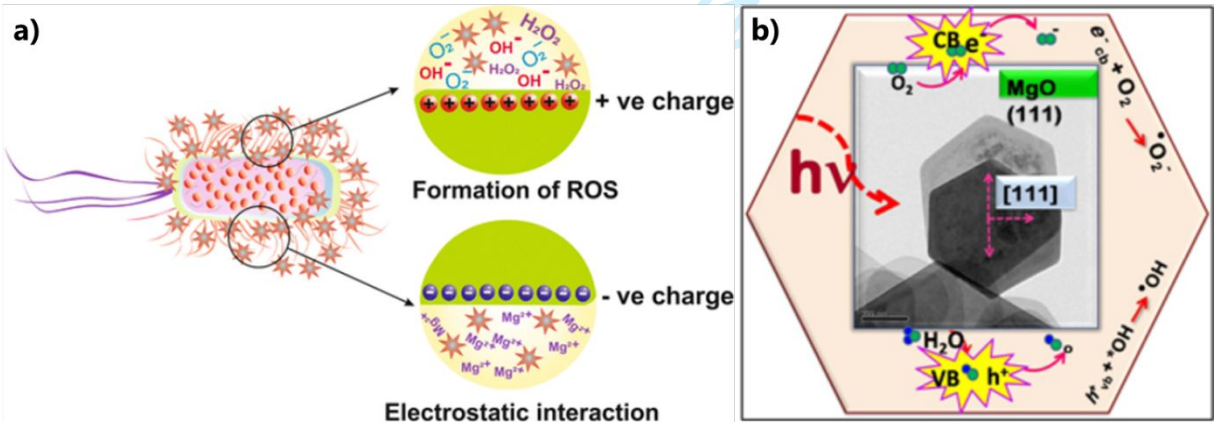

Figure 1. Graphical representation of; a) possible antibacterial mechanisms of MgO (adapted from Navik *et al*)[123], b) possible mechanisms of MgO nanoplates against *E. coli* and *B. subtilis* (adapted from Ponnuvelu *et al*)[125].